Universidade de Aveiro
2020

David Pinto Brandão

Resposta citotóxica de células de melanoma a diferentes nanopartículas de conversão ascendente e a hipertermia

Melanoma cells cytotoxic response to different upconversion nanoparticles and hyperthermia

Universidade de Aveiro
2020

David Pinto Brandão

Resposta citotóxica de células de melanoma a diferentes nanopartículas de conversão ascendente e a hipertermia

Melanoma cells cytotoxic response to different upconversion nanoparticles and hyperthermia

Dissertação apresentada à Universidade de Aveiro para cumprimento dos requisitos necessários à obtenção do grau de Mestre em Biologia Aplicada, realizada sob a orientação científica da Doutora Helena Cristina Correia de Oliveira, Investigadora Auxiliar do Departamento de Biologia da Universidade de Aveiro, e coorientação da Doutora Verónica Isabel Correia Bastos, Investigadora do Departamento de Biologia e CESAM da Universidade de Aveiro.

This work was developed within the project POCI-01-0145-FEDER-031794, financially supported funded by FEDER, through COMPETE2020 - Programa Operacional Competitividade e Internacionalização (POCI), and by national funds (OE), through FCT/MCTES (PTDC/BTM-MAT/31794/2017).

Ao Gigi por me mostrar a beleza da biologia.

o júri

presidente	Professora Doutora Etelvina Maria de Almeida Paula Figueira, Professora Auxiliar, Universidade de Aveiro
arguente principal	Doutora Fernanda de Oliveira Esteves Rosário, Investigadora Contratada, Universidade do Porto
orientador	Doutora Helena Cristina Correia de Oliveira, Equiparada a Investigadora Auxiliar, Universidade de Aveiro

agradecimentos

Gostaria de começar por agradecer as minhas orientadoras, a Professora Doutora Helena Oliveira e a Doutora Verónica Bastos, primeiro por toda a orientação técnica e científica, mas também pela forma calorosa que me acolheram neste laboratório, e por todos os momentos de riso e de amizade que foram criados ao longo deste ano caricato. Desta mesma forma agradeço a todos os elementos do grupo, por toda a bem disposição e interajuda.

Não posso, ainda assim, deixar de agradecer especialmente ao Ruben e a Parastu, a quem ao longo deste ano forjei amizades ainda mais fortes, e que estiveram sempre disponíveis para me ajudar e tirar duvidas, independentemente das horas.

Um muito obrigado a todos os meus amigos tanto de Aveiro como de Paredes, que me ajudaram sempre a manter um sorriso na cara mesmo nos piores momentos, por todos os momentos de convívio e de conversa (apesar que limitados).

À minha família agradeço-vos por me fazerem quem eu hoje sou. À minha mãe, irmão e avó um obrigado muito especial por estarem sempre ao meu lado, por me apoiarem em todas as minhas decisões, e por estarem lá quando precisava de ser levantado de novo.

Por fim, um obrigado gigante à Bruna. Obrigado por estares sempre do meu lado ao longo destes 4 anos, por me fazeres alegrares o meu dia e fazeres me rir diariamente com coisas estupidas, pelas conversas longas, tanto serias como não, principalmente durante a madrugada quando eu tinha de acordar cedo no dia seguinte. Obrigado por tudo.

palavras-chave Hipertermia, Melanoma, $NaYF_4$:Yb,Er (20/2%)@mSiO_2, Gd_2O_3:Yb,Er, Citoxidade, Nanoparticulas de conversão ascendente

Resumo

O melanoma é um dos tipos de cancro da pele mais agressivos e com uma alta taxa de mortalidade. Portanto, tem havido uma demanda crescente de novas abordagens terapêuticas para neutralizar taxas tão elevadas. A hipertermia é uma abordagem terapêutica que atua ao aumentar a temperatura dentro do tumor, desde 41 a 45 ºC. O aumento da temperatura pode interromper os processos bioquímicos das células tumorais, que por sua vez pode se traduzir em morte celular por apoptose ou necrose. No entanto, apesar de promissora, a hipertermia tem alguns obstáculos, especialmente manter uma distribuição homogênea de calor por todo o tumor. Devido às limitações desta técnica, há necessidade de criar novas formas de aplicá-la com alta eficiência.

As nanopartículas podem ser usadas para induzir hipertermia, e têm a vantagem de poderem ser ajustadas especificamente para o tumor, e dessa forma aplicar calor de dentro para fora do tumor. Vários tipos de nanopartículas têm sido usados para gerar hipertermia, mas, mais recentemente, as nanopartículas de conversão ascendente (UCNPs) têm atraído muito interesse por causa das suas características únicas.

O objetivo deste trabalho foi desenvolver as bases necessárias para aplicar a hipertermia usando UCNPs. Para atingir este objetivo, quatro linhas de células de melanoma diferentes foram utilizadas, MNT-1, B16-F10, A375 e SK-MEL-28, juntamente com 2 tipos diferentes de UCNPs, $NaYF_4$:Yb,Er (20/2%)@$mSiO_2$ ($NaYF_4$UCNPs@$mSiO_2$) e Gd_2O_3:Yb,Er (Gd_2O_3UCNPs).

Antes de cada ensaio, ambos os tipos de UCNPs foram dispersas num banho de ultrasons durante 20 minutes. A caracterização físico-química das nanopartículas foi realizada por espalhamento dinâmico de luz (DLS) para $NaYF_4$UCNPs@$mSiO_2$ tamanho das nanopartículas e morfologia também foi avaliada por microscopia eletrónica de transmissão de varrimento (STEM). Os resultados de DLS de Gd_2O_3UCNPs mostraram altos valores de diâmetro hidrodinâmico e índice de polidispersidade, indicando aglomeração das nanopartículas. Além disso, o potencial zeta apresentou baixo valor, indicando a instabilidade das nanopartículas e tendência de agregação. Os resultados de DLS de $NaYF_4$UCNPs@$mSiO_2$ mostraram valores aceitáveis de diâmetro hidrodinâmico, com baixos valores de índice de polidispersidade indicando um tamanho mais uniforme de nanopartículas. O potencial zeta de $NaYF_4$UCNPs@$mSiO_2$ indica que eles têm estabilidade incipiente a 25 µg/mL e estabilidade inferior a 100 µg/mL. A imagem e análise STEM indicaram tamanho de 77.78 ± 3.53 nm. A citotoxicidade de ambos os UCNPs foi testada pelo protocolo WST-8, com Gd_2O_3UCNPs sendo testados nas linhas celulares MNT-1 e A375, e $NaYF_4$UCNPs@$mSiO_2$ sendo testados nas quatro linhas celulares mencionadas acima. Em ambos os casos, as células foram expostas a 12,5, 25, 50, 100 e 200 µg/mL de UCNPs. Gd_2O_3UCNPs causou uma diminuição na viabilidade de A375 nas maiores concentrações após 48 horas de exposição, em comparação com o grupo de controle. $NaYF_4$UCNPs@$mSiO_2$ causou uma diminuição na viabilidade celular para todas as linhas celulares para 100 e 200 µg/mL após 24 e 48 horas, com as células MNT-1 também tendo uma diminuição da viabilidade em 25 e 50 µg/mL por 48 horas após a exposição. As células A375 têm uma diminuição da viabilidade para 50 µg/mL em 48 horas após a exposição. A internalização das $NaYF_4$UCNPs@$mSiO_2$ só aconteceu nas linhas celulares MNT-1 e SK-MEL-28. O perfil de sensibilidade à hipertermia das linhagens celulares MNT-1 e A375 foi realizado pela exposição a 43 e 45 ºC por 30, 60 e 120 minutos, e a viabilidade celular medida 24, 48 e 72 horas após a exposição por meio do ensaio MTT. Em quase todos os casos a viabilidade celular MNT-1 diminuiu com o aumento do tempo de exposição onde, após 120 minutos de exposição, a viabilidade celular ficou abaixo de 60% para todos os tempos de exposição em ambas as temperaturas testadas. Comparativamente, as células A375 expostas a 43 ºC não tiveram viabilidade inferior a 60% em todos os casos. Por fim, as células MNT-1 expostas a 45 ºC por 120 minutos apresentaram valores de viabilidade abaixo de 20% após 48 e 72 horas, enquanto, por outro lado, a viabilidade das células A375 variou de 40 a 60%, dependendo do tempo de exposição.

Este trabalho permitiu definir um intervalo de concentrações de UCNPs que podem ser usados sem comprometer a viabilidade celular, sendo bons candidatos para hipertermia induzida por radiação próxima do infravermelho para células de melanoma. Este trabalho também permitiu concluir quais temperaturas e tempos de exposição aplicar para potencializar o efeito da hipertermia em células de melanoma. As condições definidas no trabalho atual (concentrações e temperaturas de UCNPs) podem ser replicadas para gerar hipertermia desencadeada por radiação no infravermelho próximo em células de melanoma usando UCNPs.

keywords Hyperthermia, Melanoma, $NaYF_4$:Yb,Er (20/2%)@mSiO_2, Gd_2O_3:Yb,Er, Cytotoxicity, Upconversion Nanoparticles

abstract

Melanoma is one of the most aggressive types of skin cancer with a high mortality rate. Therefore, there has been an increasing demand for new therapeutic approaches to counteract such elevated rates. Hyperthermia is a therapeutic approach that works by raising the temperature inside of the tumour, ranging between 41 and 45 ºC. The temperature increase may disrupt the biochemical processes of the tumour cells, which in turn can translate into cellular death either by apoptosis or necrosis. However, this promising therapeutic therapy has some hurdles, especially regarding the homogeneous distribution of heat throughout the tumour. Because of the limitations of this technique, there is a need to create new ways of applying it with higher efficiency.

Nanoparticles can be used to induce hyperthermia, and they have the upside of being able to be fine-tuned in order to specifically target the tumour and apply heat from inside-out. Various types of nanoparticles have been used to generate hyperthermia, but more recently upconversion nanoparticles (UCNPs) have garnered a lot of interest due to their unique characteristics.

The objective of this work was to develop the groundwork needed to apply hyperthermia by using UCNPs. To achieve this objective four different melanoma cells lines were used, MNT-1, B16-F10, A375 and SK-MEL-28, along with 2 different types of UCNPs, $NaYF_4$:Yb,Er(20/2%)@$mSiO_2$ ($NaYF_4$UCNPs@$mSiO_2$) and Gd_2O_3:Yb,Er (Gd_2O_3UCNPs).

Prior to every assay, both types of UCNPs were dispersed in ultrasound bath for 20 minutes. Physicochemical characterization of nanoparticles was performed by dynamic light scattering (DLS) for $NaYF_4$UCNPs@$mSiO_2$ nanoparticles size and morphology was also assessed by

Scanning transmission electron microscopy (STEM). DLS results of Gd_2O_3UCNPs showed high values of hydrodynamic diameter and polydispersity index, indicating agglomeration of the nanoparticles. Furthermore, zeta potential showed a low value, indicating the instability of the nanoparticles and tendency to aggregate. DLS results of $NaYF_4$UCNPs@$mSiO_2$ showed acceptable values of hydrodynamic diameter, with low values of polydispersity index indicating a more uniform size of nanoparticles. Zeta potential of $NaYF_4$UCNPs@$mSiO_2$ indicate that they have incipient stability at 25 µg/mL, and lower stability at 100 µg/mL. STEM imaging and analysis indicated size of 77.78 ± 3.53 nm. Cytotoxicity of both UCNPs were tested by WST-8 protocol, with Gd_2O_3UCNPs being tested on MNT-1 and A375 cell lines, and $NaYF_4$UCNPs@$mSiO_2$ being tested on the four cell lines mentioned above. In both cases, cells were exposed to 12,5, 25, 50, 100 and 200 µg/mL of UCNPs. Gd_2O_3UCNPs caused a decrease in the viability of A375 at the highest concentrations after 48 hours of exposure, compared to the control group. $NaYF_4$UCNPs@$mSiO_2$ caused a decrease in cell viability for all cell lines for 100 and 200 µg/mL after 24 and 48 hours, with MNT-1 cells also having a decrease of viability at 25 and 50 µg/mL for 48 hours after the exposure. A375 cells have a decrease of viability for 50 µg/mL at 48 hours after the exposure. Cellular uptake of $NaYF_4$UCNPs@$mSiO_2$ only happened on MNT-1 and SK-MEL-28 cell lines. Hyperthermia sensitivity profile of MNT-1 and A375 cell lines was performed by exposure to 43 and 45 ºC during 30, 60 and 120 minutes, and cell viability measured 24, 48 and 72 hours after exposure through the MTT assay. In almost every case MNT-1 cell viability decreased with the increase of exposure time where, after 120 minutes of exposure, cell viability was below 60% for all the exposure times in both of the tested temperatures. Comparatively, A375 cells exposed to 43 ºC did not have viability lower than 60% in all cases. Finally, MNT-1 cells exposed to 45 ºC for 120 minutes showed viability values below 20% after 48 and 72 hours, while on the other hand, A375 cells viability ranged from 40 to 60%, depending on the exposure time.

This work allowed to set a range of concentrations of UCNPs that can be used without compromising cell viability, being good candidates for near-infrared induced hyperthermia to melanoma cells. This work also allowed to conclude which temperatures and exposure times to apply in order to potentiate the effect of hyperthermia in melanoma cells. The conditions defined in the current work (UCNPs concentrations and temperatures) can be replicated to generate near-infrared light-triggered hyperthermia in melanoma cells using UCNPs.

Table of contents

1. General introduction and objectives 1
1.1 Cancer 1
1.1.2 Melanoma 3
1.2 Hyperthermia 7
1.3 Lanthanide nanomaterials 11
1.3.1 Composition of UCNPs 14
1.3.2 Host material for UCNPs 14
1.3.3 Sensitizers for UCNPs 15
1.3.4 Activators for UCNPs 15
1.3.5 Synthesis of UCNPs 16
1.3.6 Bioapplications of UCNPs 17
1.3.7 *In vivo* and *in vitro* bioimaging with UCNPs 18
1.3.8 Photodynamic therapy with UCNPs 18
1.3.9 UCNPs for drug delivery 19
1.3.10 Photothermal therapy with UCNPs 20
1.4 Objectives 21
2. Materials and methods 22
2.1 Upconversion Nanoparticles 22
2.2 Physicochemical characterization of UCNPs 22
2.3 Cell culture 22
2.4 Viability assay 23
2.5 Uptake potential by flow cytometry 25
2.6 Effect of hyperthermia on cell viability 25
2.7 Statistical analysis 26
3. Results 27
3.1 Physicochemical characterisation 27
3.1.1 Dynamic light scattering of Gd_2O_3UCNPS 27
3.1.2 Dynamic light scattering of $NaYF_4$UCNPs@$mSiO_2$ 29
3.1.3 STEM analysis of $NaYF_4$UCNPs@$mSiO_2$ 31
3.2 Cell viability 32
3.2.1 Gd_2O_3UCNPS 32

3.2.2 $NaYF_4$UCNPs@$mSiO_2$ 33
3.3 Uptake 34
3.4 Temperature exposure 35
4. Discussion 37
5. Final remarks 41
6. References 42

List of figures

Figure 1: Global cancer incidence and mortality, in both sexes and ages. Adapted from [2]. 1
Figure 2: Hallmarks of cancer. Adapted from [5]. 2
Figure 3: UVA and UVB penetration on skin. Adapted from [144]. 5
Figure 4: Schematic representation of the excited-state absorption process. Adapted from [74]. 12
Figure 5: Schematic representation of the cross-relaxation upconversion process. Adapted from [74] 13
Figure 6: Schematic representation of the energy transfer upconversion process. Adapted from [74]. 14
Figure 7: Energy level diagram for UCNPs in Yb^{3+}/Er^{3+}. Adapted from [145]. 16
Figure 8: Light microscopy images of (A) MNT-1, (B) B16-F10, (C) A375 and (D) SK-MEL-28. Photos were taken with magnification of 20x and 10x combined. 24
Figure 9: Hydrodynamic diameter results of Gd_2O_3UCNPs. Results are shown as average ± standard deviation (SD). 27
Figure 10: Polydispersity index results of Gd_2O_3UCNPs. Results are shown as average ± standard deviation (SD). 28
Figure 11: Zeta potential results of Gd_2O_3UCNPs. Results are shown as average ± standard deviation (SD). 28
Figure 12: Hydrodynamic diameter results of $NaYF_4$UCNPs@$mSiO_2$. Results are shown as average ± standard deviation (SD). 29
Figure 13: Polydispersity index results of $NaYF_4$UCNPs@$mSiO_2$. Results are shown as average ± standard deviation (SD). 30
Figure 14: Zeta potential results of $NaYF_4$UCNPs@$mSiO_2$. Results are shown as average ± standard deviation (SD). 30
Figure 15: (A) Particle size distribution of $NaYF_4$UCNPs@$mSiO_2$ nanoparticles determined via image analysis with ImageJ, with an average nanoparticle size of 77.78 ± 3.53 nm. STEM images of $NaYF_4$@$mSiO_2$ nanoparticles at two different ampliations: (B) 100,000x and (C) 400,000x. 32

Figure 16: Cell viability by WST-8 protocol on MNT-1 (left) and A375 (right) cells, when exposed to Gd_2O_3 for 24 and 48 hours. Results are shown as average ± standard deviation (SD). * or # indicates significant statistical difference in relation to the control condition ($p<0.005$). 33
Figure 17: Cell viability by WST-8 protocol of MNT-1 (top left), B16-F10 (top right), A375 (bottom left) and SK-MEL-28 (bottom right) cells, when exposed to $NaYF_4$UCNPs@$mSiO_2$ for 24 and 48 hours. Results are shown as average ± standard deviation (SD). * or # indicates significant statistical difference in relation to the control condition ($p<0.005$). 34
Figure 18: Cell uptake results of MNT-1 (top left), B16-F10 (top right), A375 (bottom left) and SK-MEL-28 (bottom right) cells, when exposed to 25 and 100 µg/mL of $NaYF_4$UCNPs@$mSiO_2$ for 24 hours. Results are shown as average ± standard deviation (SD). * indicates significant statistical difference in relation to the control condition ($p<0.005$)..... 35
Figure 19: Cell viability by MTT protocol of MNT-1 cells when exposed to 43 ºC (left graph) and 45 ºC (right graph), for 30, 60, 90 and 120 minutes, 24 hours, 48 hours, and 72 hours after exposure. Results are shown as averages ± standard deviation (SD). * or # indicates significant statistical difference in relation to the control condition ($p<0.005$)..... 36
Figure 20: Cell viability by MTT protocol of A375 cells when exposed to 43 ºC (left graph) and 45 ºC (right graph), for 30, 60, 90 and 120 minutes, 24 hours, 48 hours, and 72 hours after exposure. Results are shown as averages ± standard deviation (SD). *, # or × indicates significant statistical difference in relation to the control condition ($p<0.005$)..... 36

List of tables

Table 1: Cell seeding densities used on WST-8 assay

List of abbreviations

Abs – Absorbance

dH_2O – MiliQ water

DLS – Dynamic light scattering

DMEM – Dulbecco's modified Eagle's medium

DMSO – Dimethyl sulfoxide

DNA – Deoxyribonucleic acid

FBS – Fetal bovine serum

FCM – Flow cytometry

FS – Forward scattering

Hsp – Heat shock proteins

MTT – Colorimetric 3-(4,5-dimethyl-2-thiazolyl)-2,5-diphenyl tetrazolium bromide

NIR – Near-infrared

PBS – Phosphate-buffered saline

PDI – Polydispersity index

PDT – Photodynamic therapy

PTT – Photothermal therapy

RNA – Ribonucleic acid

ROS – Reactive oxygen species

SD – Standard deviation

SS – Side scatter

STEM – Scanning transmission electron microscopy

TEM – Transmission electron microscopy

UCNPs – Upconversion nanoparticles

UV – Ultraviolet

UVA – Ultraviolet A

UVB – Ultraviolet B

UVC – Ultraviolet C

WHO – World health organization

1. General introduction and objectives

1.1 Cancer

In the current society, cancer is a serious health problem, being the second leading cause of death across the world, following cardiovascular diseases [1]. The World Health Organization (WHO) reported that in 2018 there were 18,078,957 new cases of cancer with around 9,555,027 deaths globally, with Asia and Europe, being the most affected continents (Figure 1) [2]. Cancer is a group of diseases that can be defined as a multi-cellular disease characterized by uncontrolled growth and proliferation of abnormal cells, that can present different aetiology and occurrence on various types of tissues and organs [3]. Different factors may increase the risk of developing cancer, such as genetic factors, ultraviolet rays' exposure, lifestyle among others [3].

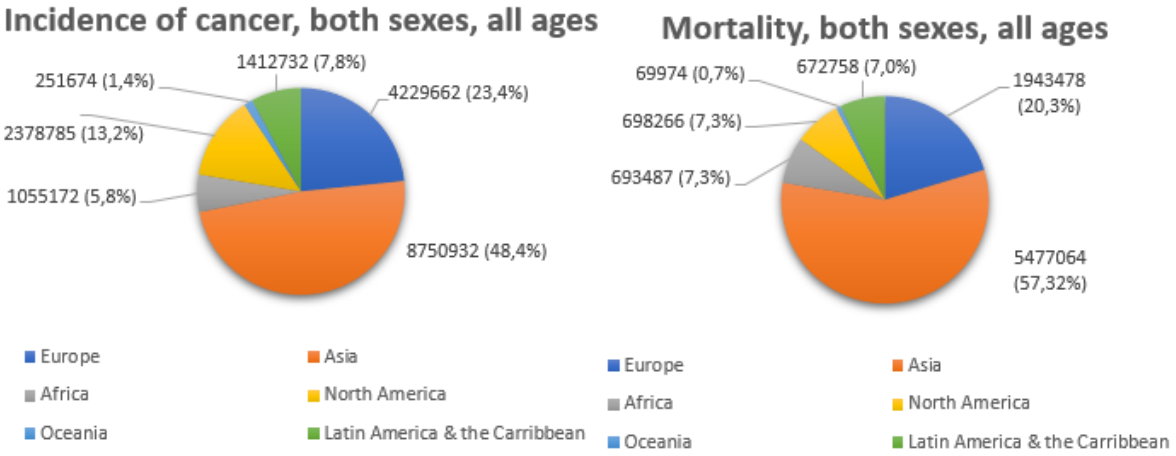

Figure 1: Global cancer incidence and mortality, in both sexes and ages. Adapted from [2].

Tumour cells vary from normal cells by having different structural and functional characteristics, which leads to genetic changes that may bolster tumorigenesis [4]. However, there are several steps required to develop malignant cells. Accordingly, in 2011, Douglas Hanahan and Robert Weinberg [5] proposed 6 necessary hallmarks (Figure 2) for such event:

1. Sustaining proliferative signalling – the most fundamental trait of cancer cells, which is its ability to maintain a chronic proliferation [5].
2. Dodging growth suppressors – Tumour suppressors normally regulate cell division, DNA repair and promote apoptosis, but mutations on the genes responsible for these suppressors are normally associated with loss of function, resulting in the inactivation of the proteins produced by these genes.
3. Resisting cell death – Apoptosis is one of the main barriers preventing cancer development. Tumour cells have different strategies to prevent circumvent apoptosis, being the loss of the TP53 tumour suppressor the most common.
4. Enabling replicative immortality – Tumour cells show an unlimited replicative potential making them immortal. In these cells, telomerases are heavily expressed, which may explain why they are immortal.
5. Inducing Angiogenesis – Tumours have the ability to create new vessels from endothelial cells and form the sprouting of existent vessels. These new vessels provide the sustenance required for tumours.
6. Activating invasion and metastasis – The ability to create secondary tumours, by deploying tumour cells from the primary tumour to invade other tissues. This is one of the main characteristics of cancer and one of its major complications.

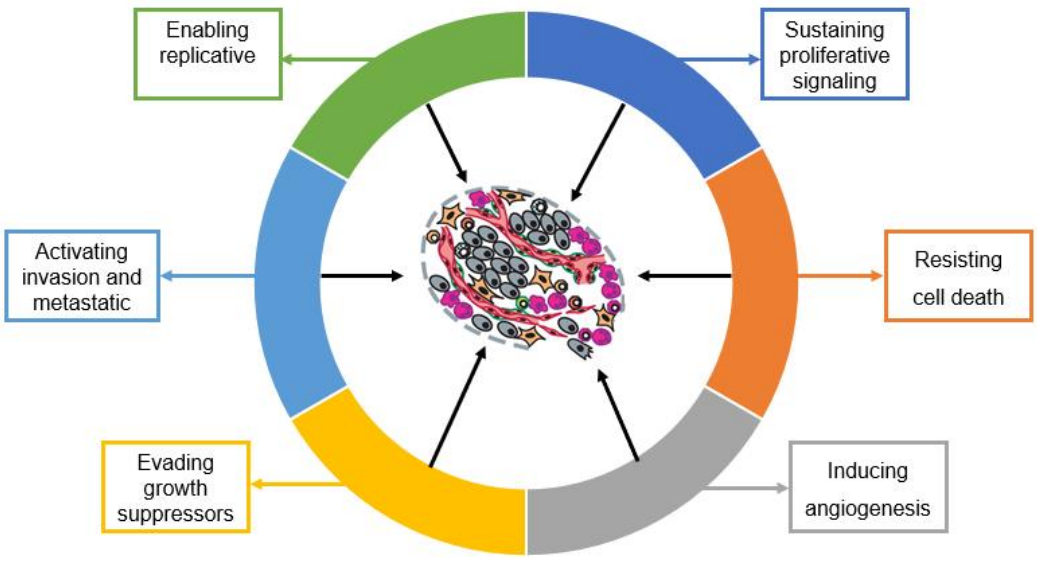

Figure 2: Hallmarks of cancer. Adapted from [5].

These hallmarks represent characteristics that normal cells go through to become tumour cells [5], and it is necessary to understand them in order to better treat cancer.

Despite its high incidence, there is not yet a cure or an effective treatment for cancer. There are some therapies that show some success, such as chemotherapy and radiotherapy, but they also affect normal cells and leads to side effects that can condition the life quality of the patient [6].

1.1.2 Melanoma

Melanoma is a type of skin cancer that develops from melanocytes, the cells responsible for producing the pigment of the skin - melanin. It is one of the most frequent types of cancer, being the most aggressive form of skin cancer with over 70% mortality rate among skin cancers [7]. Even though the mortality rate is stable or even decreasing, its incidence rate is increasing, being primarily diagnosed in young patients [8,9]. The survival rate for this type of cancer depends mainly in which stage it is diagnosed, the earlier the best, with a high survival rate of 98% with treatment by local surgery [6]. Survival rate decreases drastically according to which of the later stages it is diagnosed, especially when it reaches metastatic melanoma.

Melanoma can be divided into 2 classes based on histopathological classification: cutaneous and noncutaneous. The cutaneous melanoma can further be divided into 4 different types in relation to clinical and histological features: superficial spreading melanoma, nodular melanoma, acral lentiginous melanoma and desmoplastic melanoma [10]. Non-cutaneous melanoma can appear all over the body, in sites where melanocytes normally occur (ocular, nasopharyngeal, gastrointestinal and genitourinary) [10].

The incidence of melanoma is also influenced by factors such as genetic component, physiology, and behaviour. Since the decade of 1960, there has been an increasing incidence in Caucasian populations [11], which have a ten times higher risk of developing melanoma skin cancer than those of dark skin [12]. This type of cancer affects mostly young and middle-aged people, with the median age of

diagnosis standing at 57 years [12]. In relation to sex, there is no consistent information, with distinct studies giving different information [12].

Melanoma is normally correlated to exposure to Ultraviolet (UV) radiation. Ultraviolet radiation is classified as shortwave Ultraviolet C (UVC, 200-290 nm), midwave Ultraviolet B (UVB, 290-320 nm) and longwave Ultraviolet A (UVA, 320-400 nm) [13–15]. These radiations are differently absorbed by the ozone layer and as such, solar radiation that reaches earth surface is composed of 5 to 10% of UVB and ± 95% of UVA.

Ultraviolet A radiation and ultraviolet B radiation are able to penetrate the skin (Figure 3), with the former causing the generation of reactive oxygen species (ROS) by endogenous non-DNA chromophores, which cause cell cycle arrest and pyrimidine dimer-type DNA damage [16,17]. Reactive Oxygen Species are responsible for various cellular effects by the redox-signalling pathway and oxidative DNA damage [18]. Ultraviolet B is partially absorbed by DNA and induces the formation of DNA photoproducts. These types of damage cause a disruption of the DNA responsible for inhibiting the activity of polymerase during the replication and/or transcription of DNA [13,19].

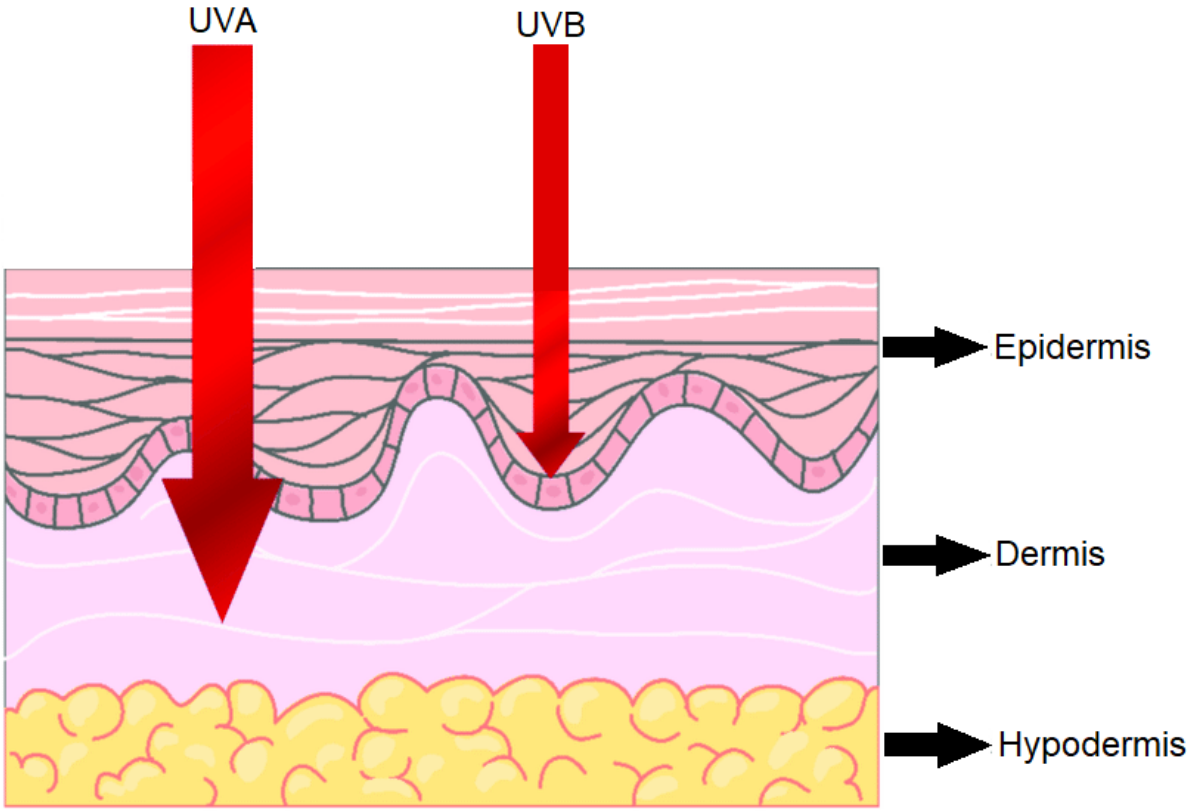

Figure 3: UVA and UVB penetration on skin. Adapted from [144].

Ultraviolet radiation has different effects on melanoma, such as causing a high mutation rate of the genetic material, mainly the conversion of C nucleotide to a T nucleotide at the TpC nucleotides [20], photolesions on DNA that codify cellular regulators (p53, EGFr, p16INK4A) which are responsible for cell growth, DNA damage repair, cell-cycle dysregulation and immunosuppression, which increases the probability of skin cancer, by upregulating the immunosuppressive cytokine IL-10 [14,18,21,22].

Familiar and individual history of melanoma are factors that increase the risk of developing this disease [23,24]. This happens through the transmission of unreliable genes regarding the repair mechanisms and cell damage-induced signalling pathways [6,25]. There are numerous genes essential for melanoma development such as cell proliferation regulation (BRAF, NRAS and NF1), DNA repair (PARP1 and ATM) and some genes in which the function is not yet determined (ARNT-SETDB1, CASP8, FTO and MX2) [24,26].

The main step to prevent melanoma is protection from UV radiation [14], with the incidence of melanoma decreasing mainly on increased awareness and regular check-ups of skin lesions such as moles [6]. Various social campaigns advocate for lower sun exposure during the most UV intense part of the day and the use of sunscreen. The incidence of melanoma is lower when the population is more informed on the effects of UV exposure [14].

Treatment for melanoma is normally conducted by surgical excision of the entire tumour. The mortality of melanoma increases with the age of the tumour, being early detection and treatment fundamental for a high survival rate.

Over the past decade, there has been an impressive clinical advance on melanoma therapy. One decade ago metastatic melanoma was considered to be a terminal disease with a survival rate lower than 5% [27], however now-a-day there has been a big increase in the survival rate due to new mechanism-based therapeutic strategies [28]. These new therapies can be grouped into 3 groups: BRAF inhibitors, MEK inhibitors and immunotherapy.

BRAF mutations are frequent in melanoma, with different incidences depending on the type of melanoma, with nodular melanoma and superficial spreading melanoma having over 50% of BRAF mutations [29–31]. For this reason, BRAF inhibitors show promise against melanoma as well as other types of cancer, by deregulating the signalling cascade RAS-RAF-MEK-ERK. Studies showed a 50% response rate to a single BRAF inhibitor and a 60-70% to a combination of 2 BRAF inhibitors [21,32,33]. MEK inhibitors, which also act by downregulating the MAPK pathway signalling also have potential to treat melanoma. Studies on MEK inhibitors showed a survival rate of 81% with an average duration of the response of 5 and a half months [34].

Immunotherapy focus on the blockage of one or two immune checkpoints, which increases the immune response of the cells. This therapy has high durability of response, but the downside is its unpredictability of response. There are currently two available therapies which target PD-1 and CTLA-4, both of which are co-inhibitory protein receptors that are expressed on the lymphocytes cell surface. Lymphocytes principal function is to preserve self-tolerance and reduce inflammatory responses in normal tissues [28,35]. This therapy has a lower survival

rate than the previous therapies mention and can also have side effects due to the disruption of normal immunological responses that can affect healthy tissues [28,36].

Even though there have been significant advances in the treatment of melanoma, there is still a need to further develop additional approaches for patients that are resistant to the currently available treatments and create new strategies to better apply the already existent therapies [28]. Other than improving the therapies already available to us, there is also a demand for new strategies to have a better range of alternatives in order to have a more fitted treatment of each patient.

1.2 Hyperthermia

Hyperthermia is a type of cancer therapy where heat is applied to a tumour mass by an external physical mean, in which the temperature inside the tumour mass increases between 41 and 48 ºC [37]. This type of therapy has long been described in the literature, but its use on medicine is somewhat new.

The first correlation between hyperthermia and its effects on cancer was noted in 1779 by Kizowitz, where he stated that high fever in patients infected purposely with malaria showed a retarded tumour growth. The first published paper on the subject would only come 90 years later, when Busch described a complete remission of face sarcoma when the patients had two erysipelas infections caused by bacteria, following a two-year disease-free survival [38]. A year later, in 1887, Bruns described complete remission in a patient with recurrent melanoma after infection of erysipelas with high fever (over 40 ºC) for several days, with an eight-year disease-free survival [39]. William B. Coley caused fever on patients by injecting them with streptococcus and noticed a correlation with the severity of the infection and the degree of regression on the tumour [40].

Hyperthermia can be divided into three different types according to the area it is applied to, with local or interstitial corresponding to the appliance of hyperthermia to the area where the tumour is located, regional hyperthermia when it is applied to a part of the body, limb, organ or a hollow cavity, and whole-body hyperthermia where body temperature is elevated to mimic a fever, with the use of warm-water immersion, heating blankets or thermal chambers[37].

The effect of hyperthermia on tumours vary according to the distinct characteristics of each tumour and its environment [37]. One way of fine-tuning the effect of heat on tumours is to modify the microenvironment where it is located since these changes can increase the response of tumours to heat [41]. Most cancer cells die when exposed to temperatures between 40 and 43 ºC, while healthy cells more likely survive [42]. Cancer cells exposed to those temperatures endure irreversible damage, which can lead to cellular death, dependent on the time and dose applied [37,43].

Pietrangeli and Mondovi [42] outlined the biochemical process of tumour cells that are affected by heat, which are:

- Inhibition of RNA synthesis, DNA, DNA repair mechanism and cell respiration,
- Strong inhibition of DNA polymerases-β crucial enzymes in multistep repair system,
- Cell membranes of tumour cells become permeable and fluid in the presence of heat,
- Heighten production of heat shock proteins (hsp) which affects thermo-tolerance and tumour immunogenicity,
- Alterations of cristae in mitochondria,
- Increased influx of reactive oxygen radicals (ROS),
- Promotion of apoptosis. All these effects, plus the microenvironment of the tumour, are responsible for the sensitivity of the tumour to heat [41,44].

Tumour growth requires new vasculature to provide nutrients [37]. This new vasculature normally is insufficient and disorganized, which results in rudimentary oxygenation and the presence of areas of hypoxia and necrosis, randomly distributed across the tumour [37]. This usually results in a hostile environment, which has negative effects on chemotherapy and radiotherapy, but it can be a boon to hyperthermia. This environment doesn't affect the action of hyperthermia on the tumour, as shown by Koutcher and Gerweck on glioblastomas [45,46], but hypoxic cells, especially the ones in acute hypoxia, are more sensitive to heat [45–47], and Hahn *et al.* showed that the metabolic state and the energy privation of these cells increases their heat sensitivity [48].

The effectiveness of hyperthermia depends on the type of tumour it is applied too since different type of cells show different sensitivity to heat treatment. Another factor that can affect cell sensitivity to heat is the phase of their cell cycle [49]. In most cases, the phase most sensitive is the mitotic phase, where heat damages the mitotic apparatus, which leads to inefficient mitosis and by consequence polyploidy. Cells in S-phase are also sensitive to hyperthermia, and in this phase, the damage is made to the chromosomes. Cells in these two phases suffer a slow mode of cell death after hyperthermia, while cells arrested in G1-phase have comparatively more heat resistant, with no damage observed microscopically, and suffer a rapid mode of death after hyperthermia [49]. The response varies according to which phase of the cell cycle the cell is in, which indicates the possibility of different cellular death mechanisms after heat exposure [50–52].

Tumours have reduced apoptosis because of an imbalance of pro-apoptotic (Bcl-2 family proteins, p53 expression) and anti-apoptotic proteins (reduced caspase activity, anomalies in the death receptors, increased endogenous inhibitors of apoptosis proteins). On the other hand, hyperthermia was reported by Ahmed and Zaidi to enhance apoptosis [53], by biochemical process's described previously, such as increasing membrane permeability of tumours, increased production of ROS, alterations of the cellular cytoskeleton [42,53,54]. Other authors have described that hyperthermia enhances apoptosis by adjusting the expression of apoptotic genes such as p52, Bcl-2 and Bax [55], and other have shown that in melanoma, hyperthermia activates a non-conventional apoptotic pathway caspases 3/7 [56].

Other than affecting the balance of apoptosis, hyperthermia also has the ability to increase the antigenic presentation of effectors cells and the production of heat shock proteins [57–60], as well as recruiting neutrophils, natural killer cells, regulatory T cells, myeloid suppressor cells and macrophages into the area of the tumour [57,58]. Hyperthermia also is able to inhibit angiogenesis, by controlling extracellular matrix degradation by inducing Plasminogen activator inhibitor-1, as demonstrated by Roca *et al.* [61].

Even though hyperthermia shows a lot of benefits, there is one major hurdle that is the homogenous heat distribution in treated tissues [62]. Current modalities of hyperthermia do not have the capability of tumour selection, and as such, they can

damage healthy tissue [63]. One way of tackling this problem is by using nanoparticles.

Different types of nanoparticles can be used in hyperthermia, such as magnetic nanoparticles, gold nanoparticles or upconversion nanoparticles. All these types of nanoparticles can be fine-tuned to target the tumour, thus circumscribe the hyperthermia to mostly the tumour alone. This ability is normally done by decorating the nanoparticles with tumour-specific molecules, such as folic acid, and as such increase the accumulation of nanoparticles inside the tumour.

Another interesting characteristic of nanoparticle use in hyperthermia is the ability to heat the tumour from the inside (inside-out hyperthermia). This ability tackles another problem of hyperthermia, that is the dissipation of heat. Normally hyperthermia is applied with an external heat source, and in this case, the blood flow inside the tumour allows for quick dissipation of the heat inside the parenchyma of the tumour [64], but when nanoparticles are used as the source of heat, they are normally placed inside the parenchyma of the tumour, overcoming this problem. The only possible problem with this type of hyperthermia is that nanoparticles might not be distributed evenly across the tumour, especially the parts further away from the vasculature where the most sensitive cells (hypoxic cells) are located [64].

Nanoparticles might be the future of hyperthermia since they can provide a more efficient and localized hyperthermia, and they also have the capability of both treating the disease as well as diagnosing it, if they are constructed in a way that allows them to be visualized by an imaging technique [64].

Even though hyperthermia is a promising field and with new discoveries and techniques still being developed, at present time the techniques available do not have a high efficiency when used alone. This inability makes it impossible to replace any of the commonly used therapies to treat cancer, but they have the ability to improve other therapies, such as radiotherapy and chemotherapy, by enhancing the cell-killing effect of cytotoxic drugs and/or radiation [49]. Because of this, there is a need to create new techniques to apply hyperthermia is a more controlled way and with high efficiency. One possibility is the use of nanoparticles, especially upconversion nanoparticles since they have special characteristics that will be discussed in the next topic.

1.3 Lanthanide nanomaterials

Nanoparticles are solid colloidal particles with size ranging from 1 to 100 nm [65]. They are composed of 3 layers: (i) surface layer, that can be functionalized, (ii) shell layer, which is chemically unlike the core of the nanoparticles and (ii) the core, which si the central part of the nanoparticle [66]. Nanoparticles can be made from a wide variety of meterials, such transitional metals, carbon, metal oxides and inorganic materials. They can be synthesized by various chemical and physical methods [67], and they are classified according to their dimensionality, morphology, composition, uniformity and agglomeration [67,68].

Lanthanides are a group of rare earth chemical elements where the atomic numbers range between 57 and 71 and are located in the sixth period and the IIIB group of the periodic table. They range from lanthanum and lutetium. These elements plus scandium and yttrium are also called rare earth elements. This term was first coined by the chemist Johan Gadolin in 1794, because of the low concentration on rare minerals [69]. The lanthanides were first discovered in 1787 when a mineral was identified in a Swedish town named Ytterby [70]. This mineral was then separated into the various types of lanthanide elements, and then yttria, an impure form of yttrium oxide, was obtained by Professor Gadolin in 1794 [69]. Over the past two centuries, the further development of lanthanide chemistry has led to the application of these elements in different fields such as agriculture, chemical industry and biomedicine [71–73].

Lanthanides have inherent luminescence which derives from f-f electron transitions in the $4f$ sub-shell, which provide exclusive properties for optical imaging. In recent years, lanthanide luminescence has been gaining a lot of consideration, in particular when doped in inorganic hosts with the size on the nanometre region [74]. The luminescence typically occurs from direct excitation that provokes an excited stated, which is followed by emission and return to the ground state. It is necessary, though, a suitable excitation source, in which the wavelength is resonant with the energy gap between the ground state and the excited states [74].

Luminescence emission of lanthanides can be achieved by a process known as upconversion. This is a process where the excitation light, a low energy near-

infrared (NIR), is converted into higher energy wavelengths shorter than the excitation source, that covers a broad region of the ultraviolet, visible and NIR [75]. In this case, the absorption of the photons is sequential and not simultaneous [76], and it requires that the excitation is provided by ultrafast (femtosecond) pulse lasers. The sequential and step by step absorption of NIR photons is possible by the intermediate excited states, which have lifetimes in the µs to ms range, and therefore allow the excitation to the final energy state of the photons and the generation of a higher energy photon [74].

There are three main mechanisms in which upconversion occur:

- Excited-state absorption – Involves a single ion and is the successive absorption of two photons by a single LN^{3+} ion [74] (Figure 4);

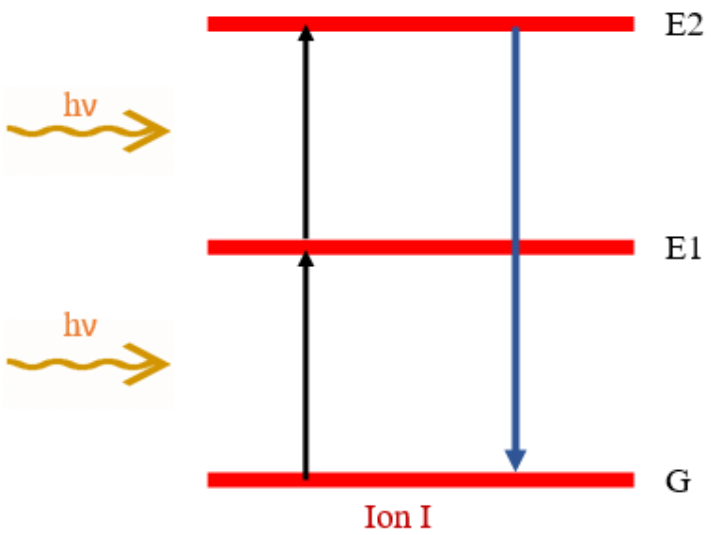

Figure 4: Schematic representation of the excited-state absorption process. Adapted from [74].

- Cross-relaxation upconversion – Two identical neighbouring ions are excited from the ground state to intermediate excited state by ground-state absorption, and then one ion returns to the ground state while the other is promoted to upper emitting level (Figure 5).

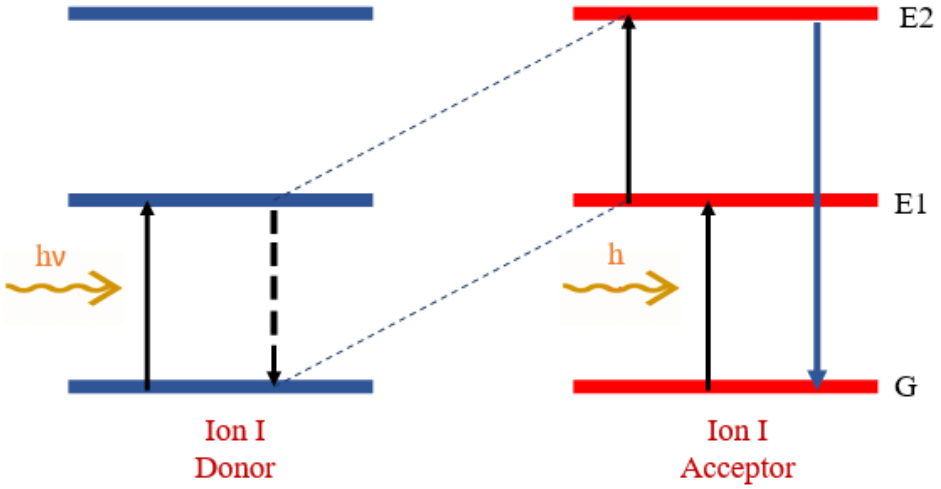

Figure 5: Schematic representation of the cross-relaxation upconversion process. Adapted from [74]

- Energy transfer upconversion – Occurs in co-doped materials, in which successive energy transfer from a donor ion to an acceptor ion happens. The donor ions are excited to intermediate states by ground-state absorption, and then energy transfer from the donor ions to the acceptor ions result in the promotion to its intermediate state. Afterwards, a second energy transfer occurs and promotes the acceptor ion to its emitting state (Figure 6).

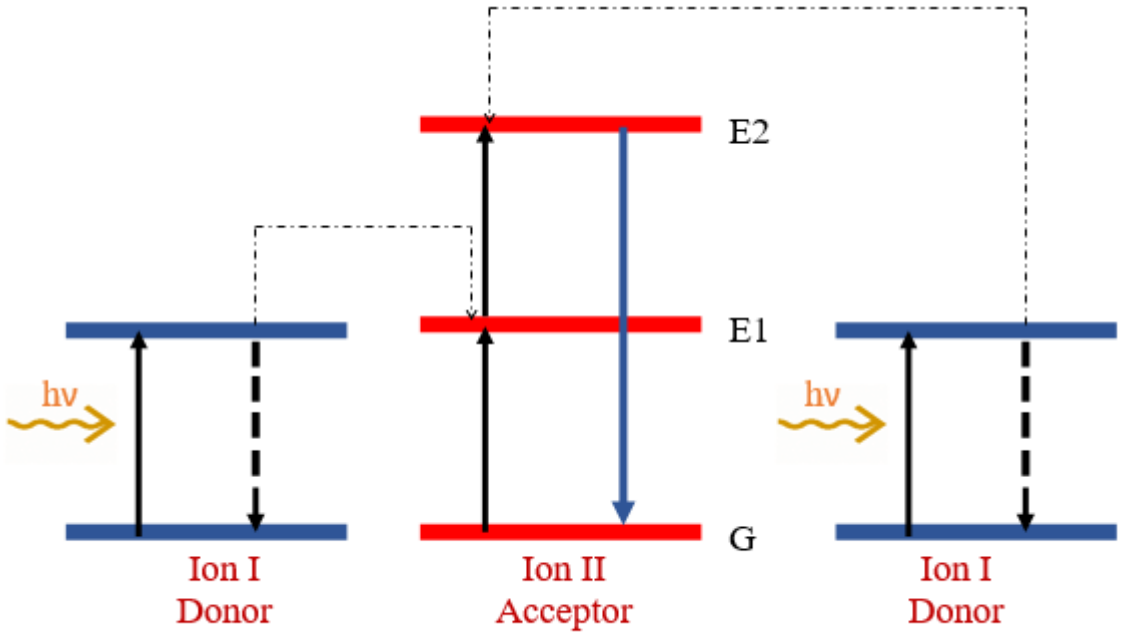

Figure 6: Schematic representation of the energy transfer upconversion process. Adapted from [74].

1.3.1 Composition of UCNPs

Upconversion nanoparticles are composed of a host material, sensitizers and activators. Normally UCNPs are composed of an inorganic host doped with Ln^{3+} ions. These ions should be less than 10 Å apart in order to have the most efficient method of upconversion [74,77].

1.3.2 Host material for UCNPs

Host material absorption should be as low as possible, so they should be transparent in the NIR and visible wavelengths region, as well as low energy phonons. With these conditions luminescence of the nanoparticles should be maximized.

To this date, the best host materials belong to the fluorides family, since they normally have phonon energy levels of bellow 500 cm^{-1} and are highly chemically stable [78]. For the mention reasons, the most popular host has been $NaREF_4$, such as $NaYF_4$ [79–82], $NaGdF_4$ [83,84], $NaLuF_4$ [85].

There are two different structural phases of $NaREF_4$ UCNPs, the cubic phase (α-) and the hexagonal phase (β-), with the latter being the most efficient phase due to its crystal structure [86].

1.3.3 Sensitizers for UCNPs

Sensitizers should have a high absorption cross-section which matches the energy levels and excitation wavelength of the activator. Ytterbium (Yb^{3+}) fulfils all the previous conditions, with his energy level only having one excited state ($^2F_{5/2}$) that resonates with 980 nm wavelength light, making him the best choice for a sensitizer [74].

With Yb^{3+} a 980 nm laser is applied as the excitation source in order to match the $^2F_{7/2} \rightarrow ^2F_{5/2}$ transition. The gap between $^2F_{7/2}$ and $^2F_{5/2}$ resonates with energy gaps of different excited states of ions normally used as activators, such as Er^{3+} [74] (Figure 7).

1.3.4 Activators for UCNPs

Activators are characterized by having homogeneously distributed energy levels that have an energy separation equal to the sensitizer emission. When sensitizers are excited, activators obtain energy from the sensitizers close by in order to promote transitions to higher energy levels. Based on this Er^{3+}, Tm^{3+} and Ho^{3+} are excellent activators, especially Er^{3+} and Tm^{3+}, due to the cascading arrangement of their energy levels [87].

Erbium ion (Er^{3+}) has a higher upconversion efficiency due to the energy gaps of the first transition ($^4I_{15/2}$ to $^4I_{11/2}$) and the second transition ($^4I_{11/2}$ to $^4F_{7/2}$)).

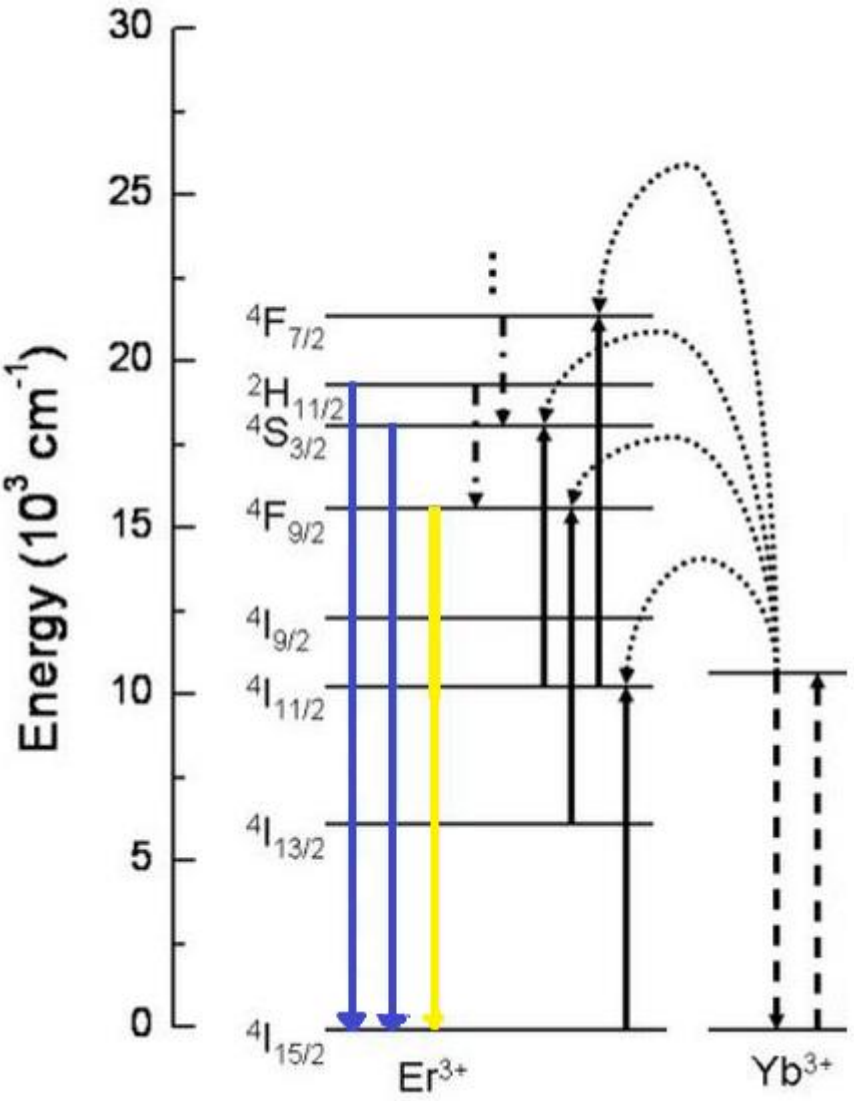

Figure 7: Energy level diagram for UCNPs in Yb^{3+}/Er^{3+}. Adapted from [145].

1.3.5 Synthesis of UCNPs

In order to use UNCPs for bioimaging and therapeutic applications, there is a need to have a controlled synthesis of monodispersed particles. There are several methods to achieve monodispersed UCNPs such as microwave [88,89], hydrothermal/solvothermal [90,91], thermal decomposition (thermolysis) [92,93], between others.

Of the three mentioned methods, thermal decomposition with metal trifluoroacetate as precursors is the most common route to synthesize monodispersed UCNPs of high quality. This method is based on the chemical

decomposition caused by heat and was first used to the synthesis of highly dispersed LaF_3 in 2005 [94]. In the following year, this approach was later modified and extended to the synthesis of $NaYF_4$ nanoparticles [92].

Over the last few years, a new type of UCNPs has been developed, hollow UCNPs. This type of UCNPs can be used effectively has storage tools or delivery of therapeutic agents.

1.3.6 Bioapplications of UCNPs

Various optical imaging techniques make use of particles, such as organic dyes or semiconductor quantum dots, for biological applications, however, these particles require emission at longer wavelengths and excitation by high energy radiation in the UV or visible region [95,96]. This type of wavelengths come with their own flaws when applied in biological tissues, because they have a lower penetration as a result of scattering processes and diverse absorption, low contrast because of background fluorescence, tissue damage due to phototoxicity of UV light and photobleaching restricting their use (in organic dyes) [74]. Due to these limitations, there is a need to produce other optical imaging techniques that are able to overcome these limitations, granting a reliable and efficient optical bioimaging. Hence, UCNPs can overcome these obstacles, making them a very promising luminescent probe for biological applications [97–99].

Upconversion nanoparticles main advantage lies in their capability of being excited by NIR photons and an emission range from UV light to NIR. Other than this advantage they also have an exceptional penetration depth *in vivo*, low cyto- and phototoxicity and a reduced background autofluorescence from the biological structures. Due to these reasons, UCNPs have shown a compelling potential for bioimaging and cancer therapy applications. In bioimaging, they have been used for *in vitro* imaging [100], *in vivo* imaging [101,102], and have been combined with other bio-imaging techniques, such as positron emission tomography [103] and diffuse optical tomography [104]. As for cancer therapy, the luminescence of these particles can be exploited for other applications, such as photodynamic therapy [105,106], drug delivery [107–109] and photothermal therapy [110,111].

1.3.7 *In vivo* and *in vitro* bioimaging with UCNPs

Since the first synthesized, UCNPs have been applied in *in vitro* (cells) and *in vivo* (small animals) imaging. In *in vitro* imaging, cytotoxicity and water dispersion pose as the main obstacles to the effective use of UCNPs. Vetrone *et al.* used polyethyleneimine capped $NaYF_4$:Er^{3+}, Yb^{3+} UCNPs to study intracellular imaging of HeLa cells, with the results showing a repositioning of UCNPs inside the cell with an increase in incubation time, showing a promising application for real-time imaging of cellular dynamics [112]. Cellular cytotoxicity and cellular imaging were tested by Shan *et al.*, by preparing hydrophobically bonded $NaYF_4$ UCNPs with amino and carboxyl groups, which showed low cytotoxicity and uptake confirmed by TEM image analysis on HOS cells [113].

Regarding *in vivo* imaging, Lim *et al.* first reported that *Caenorhabditis elegans* (roundworm) were injected with UCNPs. In this experiment, luminescence from the intestines of the worms was reported, with no cytotoxicity reported in a 24 hours period [114]. In 2008, Zhang *et al.* used rats as models and subcutaneously injected UCNPs. Compared to the control group, which was injected subcutaneously with inorganic green-emitting quantum dots, the rats injected with UCNPs showed a stronger luminescence [115].

It is also possible to study multimodal imaging by combining UCNPs with other imaging techniques, such as ultrasound imaging, magnetic resonance imaging, positron emission tomography, computed tomography [116–118].

1.3.8 Photodynamic therapy with UCNPs

Photodynamic therapy (PDT) is a clinical treatment where a light-sensitive drug, a photosensitizer, causes controlled cell death in the presence of light in a specific wavelength. In this technique, the photosensitizer is introduced in the cells, then it is excited by a light at a specific wavelength, which depends on the type of photosensitizer. After the excitation, energy is transferred to molecular oxygen in is surroundings, which generates reactive oxygen species (ROS) that can trigger cell death [119,120].

Photodynamic therapy has some limitations, such as the need for UV or visible light to excite the photosensitizer. These types of light have low penetration on biological tissues and cause cellular damage, so in order to overcome this obstacle, UCNPs can be used.

Upconversion nanoparticles can be excited by near-infrared light and emit in the UV or visible photons, which can be used to activate photosensitizers and subsequently produce ROS leading to cell death. For this reason, the combination of UCNPs and PDT has gained attention.

Several studies of the combination of UCNPs and PDT have been done, most using $NaYF_4$:Er^{3+}, Yb^{3+}, with one photosensitizer, for example, Rose Bengal hexanoic acid [121], or more, when the absorption bands match different upconversion emissions of the UCNPs [106]. Zhang *et al.* [119] published the first work that combined UCNPs and PDT, that proved that this concept works. X. M. Liu *et al.* also worked with this combination, having a $NaYF_4$:Tm^{3+}, Yb^{3+}/Er^{3+}, Yb^{3+} (core/shell) nanoparticle, which was used as a donor to monomalonic fullerene. Their results showed higher efficiency of this treatment [122].

1.3.9 UCNPs for drug delivery

Upconversion nanoparticles have also been applied to drug delivery therapy. At present time there are different nanostructures for drug delivery, such as nanoparticles, micelles, liposomes, *etc.* [123]. All the different structures have a size distribution between 10 and 100 nm, in order to prevent discharge by the reticuloendothelial system [124], allowing them to be in the bloodstream for longer periods [125].

The present time nanostructures can be improved by adding optical tagging, in order to see their distribution *in vivo* and have a better monitoring service of the treatment. Upconversion nanoparticles can achieve this, making them of great interest in drug delivery systems.

There are 3 main techniques of drug-delivering with the use of UCNPs:

- Porous shell to load the drug and slowly release it by diffusion or erosion of the shell. When UCNPs are used like this, they normally are

encapsulated in a mesoporous silica shell, where the drug is loaded by capillarity, and are slowly released.

- Hollow nanoparticles with a mesoporous silica shell, where the drug is loaded inside the nanoparticle. Hollow UCNPs release the drug as they are excited, normally having more cytotoxicity than drug delivery without nanoparticles.
- Upconversion nanoparticles can be coated with an amphiphilic polymer, which transfers hydrophobic UCNPs to their biological environment. In this case, drug delivery is normally pH-sensitive, making them more specific.

1.3.10 Photothermal therapy with UCNPs

Photothermal therapy (PTT) treatment works by inducing high temperature to kill cells [126]. This type of therapy has the advantage of selectivity towards cancer cells since tumour cells are more sensitive to heat than normal cells [127].

In order to achieve high temperatures inside the cells, there has to be an efficient mechanism to transform the energy from a light source (normally a laser because of its monochromaticity and high power) by optical absorption.

This therapy normally uses noble metals, such as gold or silver, since they have a strong surface plasmon resonance absorption and light emission that releases heat. Upconversion nanoparticles are normally used with other nanoparticles for PTT, since they can be excited by NIR light and emit radiate in the wavelength that excites other nanoparticles, such as gold nanoparticles, to induce heat. This option has been explored by other groups, such as the work developed by Qian *et al.* that used gold decorated UCNPs ($NaYF_4:Er^{3+}$, $Yb^{3+}/NaYF_4$/silica (core/shell/shell)), which showed that BE(2)-C cancer cells were killed after irradiation with a laser at 980 nm[128].

Besides combining UCNPs with other nanoparticles, several studies showed that UCNPs with a silica shell ($NaYF_4@SiO_2$) can also be used the source of heat. Carrasco *et al.* showed that neodymium ions (Nd^{3+}) coated UCNPs were able to irradicate a tumour from a mouse by increasing the temperature inside the tumour to around 47 ºC [129]. The work by Zhang *et al.* [130]also showed an increase in

temperature of $NaYF_4:Er^{3+}/Yb^{3+}$ when irradiated with a 980 nm laser, revealing good potential for PTT.

With the possibility of using UCNPs alone to cause hyperthermia, and their ability to act both as the source of heat and as a sensor for imaging techniques, it makes them a prime candidate to further develop hyperthermia therapy, until it can be regularly applied in medicine.

1.4 Objectives

In this work, the main objective was to develop the groundwork to apply hyperthermia by UCNPs. To achieve this goal the specific aims were:

- Assess and analyse the physicochemical properties of two different types of upconversion nanoparticles;
- Verify the biocompatibility of upconversion nanoparticles in four different melanoma cell lines;
- Evaluate the sensitivity of melanoma cells to hyperthermia by studying the effects of different temperatures and exposure times.

2. Materials and methods

2.1 Upconversion Nanoparticles

In this work two different nanoparticles were used: $NaYF_4$:Yb/Er(20/2%)@$mSiO_2$ ($NaYF_4$UCNPs@$mSiO_2$), provided by Dr. Maysoon Saleh from Dr. Ute Resch-Genger group, from Federal Institute for Material Research testing (BAM), Berlin, Germany, and Gd_2O_3:Yb/Er (Gd_2O_3UCNPs) provided by Dr. Mengistie Debasu and Professor Luís Carlos from CICECO – Aveiro Institute of Materials, Department of Physics, Universidade de Aveiro.

2.2 Physicochemical characterization of UCNPs

Morphology and size were analysed by scanning transmission electron microscopy (STEM) using a 200 kV Hitachi HD-2700 (Hitachi High-Technologies Europe GmbH, Germany) STEM microscope equipped with energy-dispersive X-ray spectroscopy and secondary electron detectors. Samples for STEM analysis were prepared by evaporating 10 µL of nanoparticle solution on a grid.

The hydrodynamic diameter and polydispersity index (PDI) of the nanoparticles were measured by dynamic light scattering (DLS) and the zeta potential was assessed by electrophoretic mobility. Both measurements were performed using a Zetasizer Nano ZS (Malvern Instruments, UK), which uses multi-scatter laser diffraction to determine the size of the nanoparticles and its agglomeration.

Prior to any protocol, nanoparticles were dispersed by ultrasonic bath for 20 minutes.

For all the experiments UCNPs were dispersed in Mili-Q water and DMEM medium at 25 and 100 µg/mL, with 3 replicas each.

2.3 Cell culture

The MNT-1 cell line (a tumorigenic immortalized highly pigmented human melanoma cell line) was provided by Dr Manuela Gaspar (iMed.ULisboa, Portugal),

while B16-F10 (a tumorigenic immortalized *Mus musculus* skin cell line) A375 (amelanotic human epithelial skin cell line) and SK-MEL-28 (a lightly pigmented human melanoma cell line) were purchased from ATCC. Cells were cultured in DMEM (Dulbecco's modified Eagle's medium) supplemented with 10% fetal bovine serum (FBS), 2mML-glutamine, 100 U/mL penicillin, 100 µg/mL streptomycin and 2.5 µg/mL fungizone, at 37 ºC in 5% CO_2 humidified atmosphere.

Cells were observed daily to verify confluence, morphology and the presence of contaminants by an inverted phase-contrast microscope Nikon Eclipse TS100 (Tokyo, Japan). When the confluence of the culture reached 80%, the subculture was performed. Briefly, the old medium was removed, the cells were washed with PBS to remove any impurities. Afterwards, trypsin was added to detach the cells from the flask and was incubated for 5 minutes at 37 ºC, 5% CO_2. After the incubation, medium was added to the flask, twice the volume of trypsin, in order to inactivate trypsin. Subsequently, the cells were counted in a haemocytometer and the desired number of cells were seeded into a new flask.

2.4 Viability assay

Cell viability of all the aforementioned cell lines was determined by the colourimetric WST-8, which is based on the biopreduction of tetrazolium salt WST-8 in the presence of an electron carrier, produzing a water-soluble formazan. Cells were seeded in 96-well plates, at densities described in table 1, and cultured as previously described. Cell viability was assessed in cells exposed to UCNP dissolved in medium at 200, 100, 50, 25 and 12,5 µg/mL, previously dispersed in ultrasonic bath for 20 minutes. Cell viability was measured after 24 h and 48 h. The medium was removed and substituted by 110 microliters of WST-8 at 10% in medium, and incubated for 2 h at 37 ºC, 5% CO_2.

Table 1 Cell seeding densities used on WST-8 assay

	24 HOURS	48 HOURS	72 HOURS
MNT-1	35000 cells/mL	25000 cells/mL	15000 cells/mL
B16-F10	25000 cells/mL	10000 cells/mL	5000 cells/mL
A375	35000 cells/mL	25000 cells/mL	20000 cells/mL
SK-MEL-28	50000 cells/mL	20000 cells/mL	10000 cells/mL

The optical density of WST-8 was measured at 450 nm in a microtiter plate reader (Synergy HT Multi-Mode, BioTek, Vinooski, VT), and the cell viability was calculated as:

$$Cell\ viability = \left(\frac{(Sample\ Abs - Blank\ Abs)}{(\text{Control Abs} - \text{Blank Abs})}\right) * 100$$

Two independent assays were performed with 4 replicates each, comparing the results with the control group (no exposure).

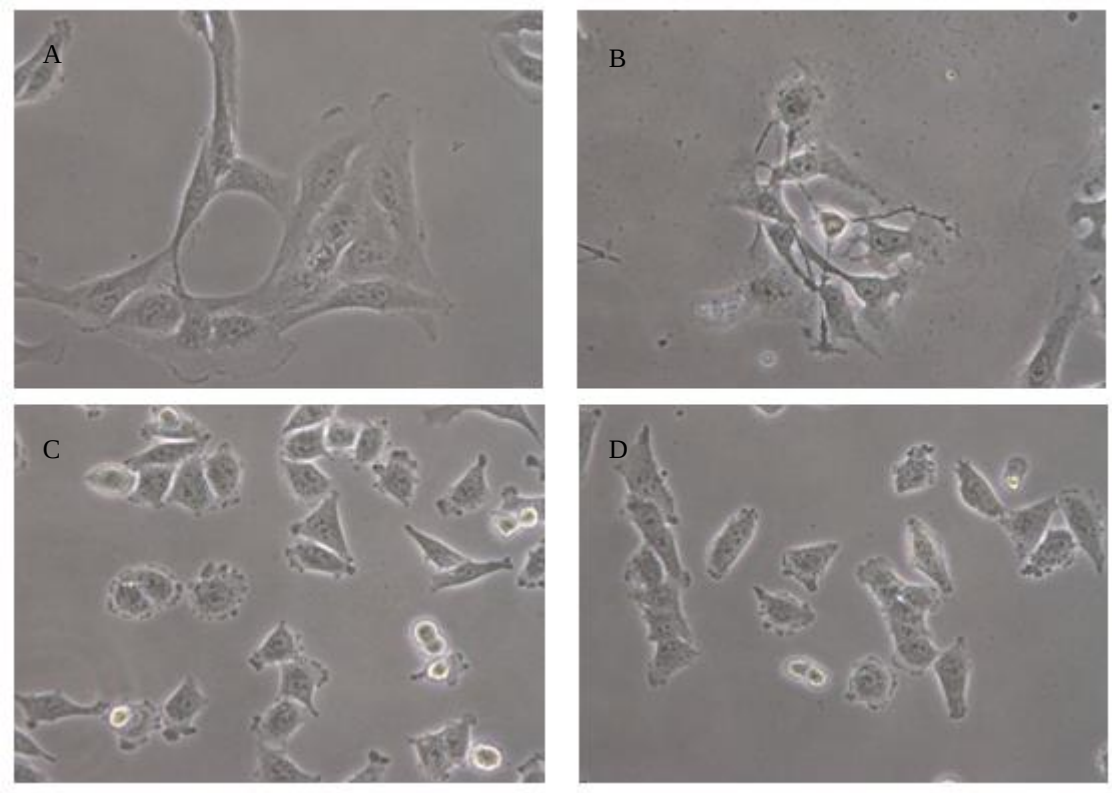

Figure 8: Light microscopy images of (A) MNT-1, (B) B16-F10, (C) A375 and (D) SK-MEL-28. Photos were taken with magnification of 20x and 10x combined.

2.5 Uptake potential by flow cytometry

Uptake potential of MNT-1, B16-F10, A375 and SK-MEL-28 cells, at the same concentration as the WST-8 assay, was determined by flow cytometry, as described by Suzuki *et al.* (2007). Briefly, cells were seeded in 24-well plates and after UCNP exposure they were trypsinized, collected to Eppendorf tubes and analysed by flow cytometry (FCM). Both parameters, forward scatter (FS), providing information on the particle's size, and side scatter (SS), providing information on the complexity of particles, were measured in an Attune® Acoustic Focusing Cytometer (TermoFisher Scientific) equipped with a 488 nm laser. For each sample, at least 100000 cells were analysed.

2.6 Effect of hyperthermia on cell viability

To evaluate the effect of temperature, cell viability was assessed by the colourimetric 3-(4,5-dimethyl-2-thiazolyl)-2,5-diphenyl tetrazolium bromide (MTT) assay, which is based on the bioreduction of the tetrazolium dye MTT by oxireductases enzymes, produzing insoluble formazan. Briefly, cells were seeded in 96-well plates and cultured as described previously in WST-8 viability assay, where instead of adding UCNPs, the temperature effects were assessed in cells exposed to 43 and 45 ºC for 30, 60 and 120 minutes. Cell viability was measured after 24 h, 48 h and 72 h. The medium was removed and substituted by 50 microliters of MTT and incubated for 4 hours at 37 ºC, 5% CO_2. Then, MTT was removed and 150 microliters of dimethyl sulfoxide (DMSO) were placed in each well and were agitated in the dark for 2 hours.

The optical density of MTT was measured at 570 nm in a microtiter plate reader (Synergy HT Multi-Mode, BioTek, Vinooski, VT), and the cell viability was calculated as:

$$Cell\ viability = \left(\frac{(Sample\ Abs - Blank\ Abs)}{(\text{Control Abs} - \text{Blank Abs})}\right) * 100$$

Results were compared with the control group (without exposure).

2.7 Statistical analysis

The results are reported as mean ± standard deviation (SD) of 4 technical replicates in each of the 2 independent experiments. For all assays one-way ANOVA was performed, followed by Dunnet and Dunn's tests (as a parametric and non-parametric test, respectively), using Sigma Plot 11.0 software (Systat Software Inc.). The differences were considered statistically significant for $p < 0,05$.

3. Results

3.1 Physicochemical characterisation

3.1.1 Dynamic light scattering of Gd_2O_3UCNPS

Physicochemical characterization by DLS of Gd_2O_3UCNPs, after dispersion in ultrasonic bath for 20 minutes showed that in water the average hydrodynamic diameter (Dh) was near 1840 nm, while in DMEM medium the Dh values were considerably lower, respectively 306 nm and 560 nm for the suspensions of 25 µg/ml and 100 µg/ml (Figure 9).

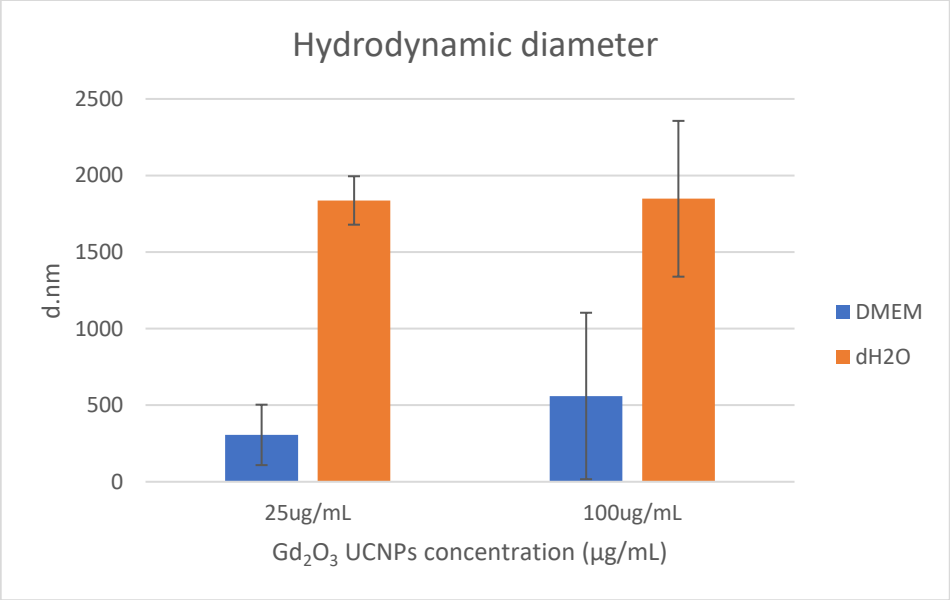

Figure 9: Hydrodynamic diameter results of Gd_2O_3UCNPs. Results are shown as average ± standard deviation (SD).

Hydrodynamic diameter results (Figure 9) showed higher values than expected, being the dispersion in dH_2O the highest. These results might be explained by agglomeration of the nanoparticles.

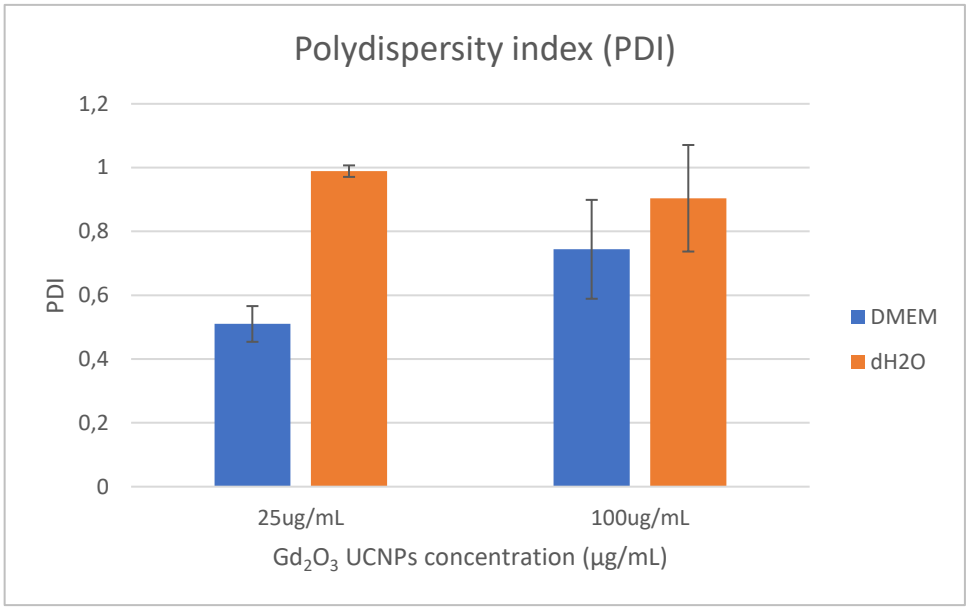

Figure 10: Polydispersity index results of Gd_2O_3UCNPs. Results are shown as average ± standard deviation (SD).

The values of polydispersity index (PDI) for Gd_2O_3UCNPs (Figure 10) in water were 0.99 and 0.90, respectively for 25 and 100 µg/ml suspensions. In DMEM medium PDI values were lower than in water, being respectively 0.51 and 0.74 for the 25 and 100 µg/ml suspensions .

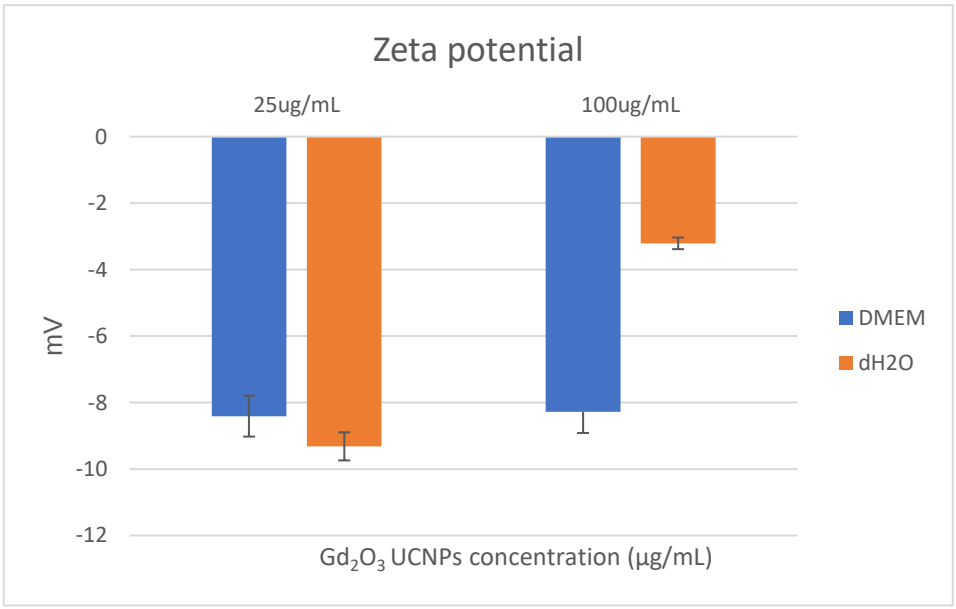

Figure 11: Zeta potential results of Gd_2O_3UCNPs. Results are shown as average ± standard deviation (SD).

Zeta potential values of Gd_2O_3UCNPs nanoparticles (Figure 11) in dH_2O were -9.32 and -3.21 for 25 and 100 µg/mL, respectively. In DMEM medium zeta potential was more uniform, with -8.41 for 25 µg/mL and -8.28 µg/mL.

3.1.2 Dynamic light scattering of $NaYF_4$UCNPs@$mSiO_2$

Physicochemical characterization by DLS of $NaYF_4$UCNPs@$mSiO_2$, after dispersion in ultrasonic bath for 20 minutes.

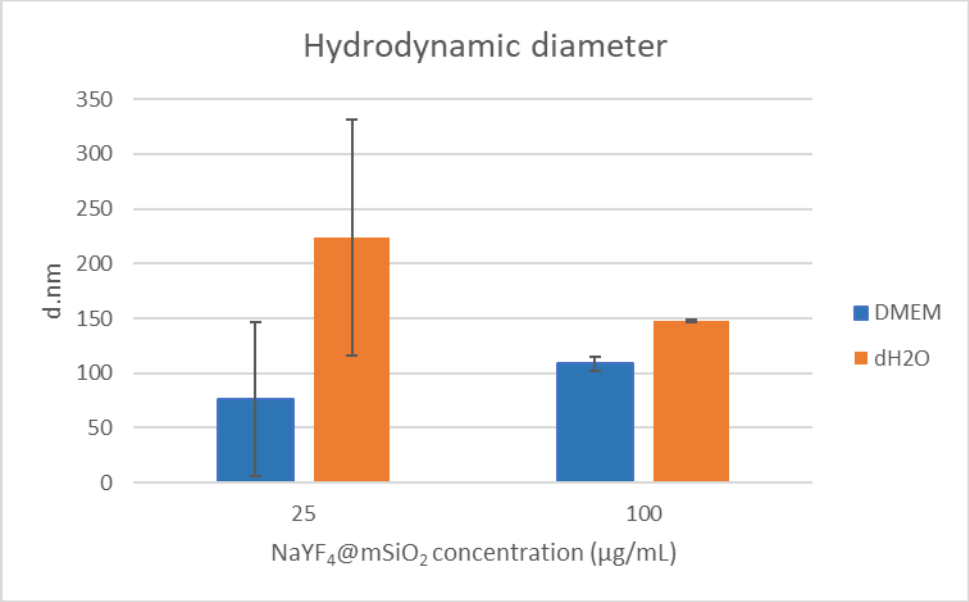

Figure 12: Hydrodynamic diameter results of $NaYF_4$UCNPs@$mSiO_2$. Results are shown as average ± standard deviation (SD).

The average hydrodynamic diameter (Dh) for $NaYF_4$UCNPs@$mSiO_2$ was 76.68 and 108.7 nm in DMEM medium, for 25 and 100 µg/mL respectively (Figure 12).

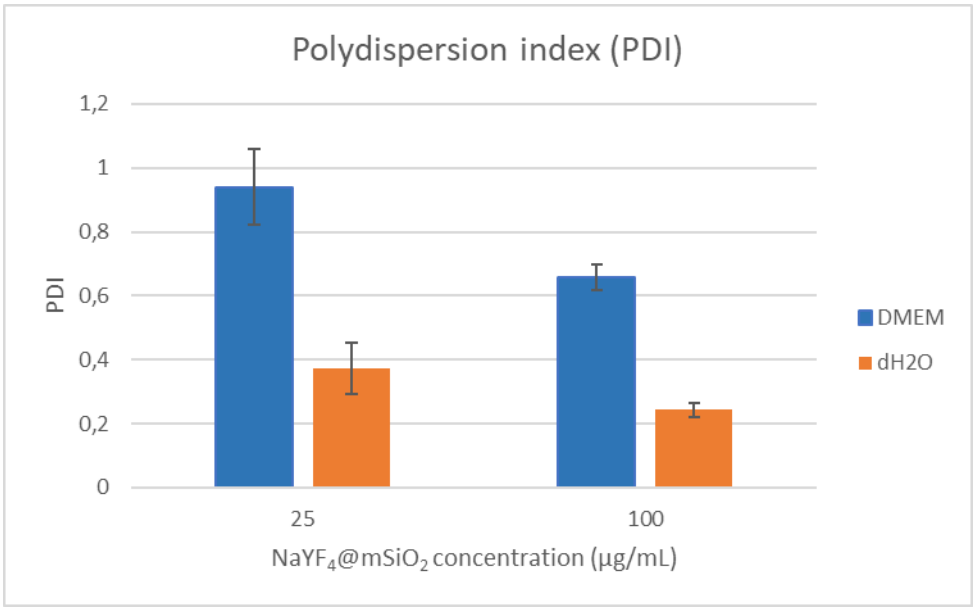

Figure 13: Polydispersity index results of $NaYF_4$UCNPs@$mSiO_2$. Results are shown as average ± standard deviation (SD).

Polidispersity index values for $NaYF_4$UCNPs@$mSiO_2$ (Figure 13) in water were 0.373 and 0.244 for 25 and 100 µg/mL, respectively. In DMEM medium PDI values were 0.94 for 25 µg/mL and 0.658 for 100 µg/mL.

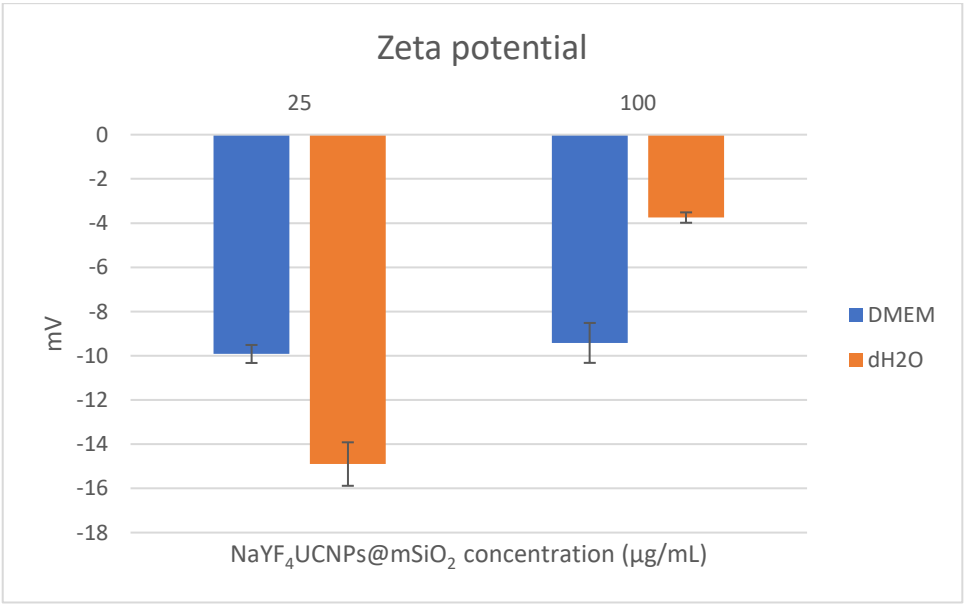

Figure 14: Zeta potential results of $NaYF_4$UCNPs@$mSiO_2$. Results are shown as average ± standard deviation (SD).

Zeta potential for $NaYF_4$UCNPs@$mSiO_2$ nanoparticles (Figure 14) in dH_2O were -14.9 and -3.75 for 25 and 100 µg/mL, respectively. In DMEM medium zeta potential was more uniform, with -9.92 for 25 µg/mL and -9.42 for µg/mL.

3.1.3 STEM analysis of $NaYF_4$UCNPs@$mSiO_2$

Size and morphology of $NaYF_4$UCNPs@$mSiO_2$ was analysed by scanning transmission electron microscopy. As observed in Figure 15 $NaYF_4$UCNPs@$mSiO_2$ showed monodispersed and uniform spherical morphologies, being each core well encapsulated with a silica shell (Figure 15 B and C). Their average size was 77.88 ± 3.53 nm.

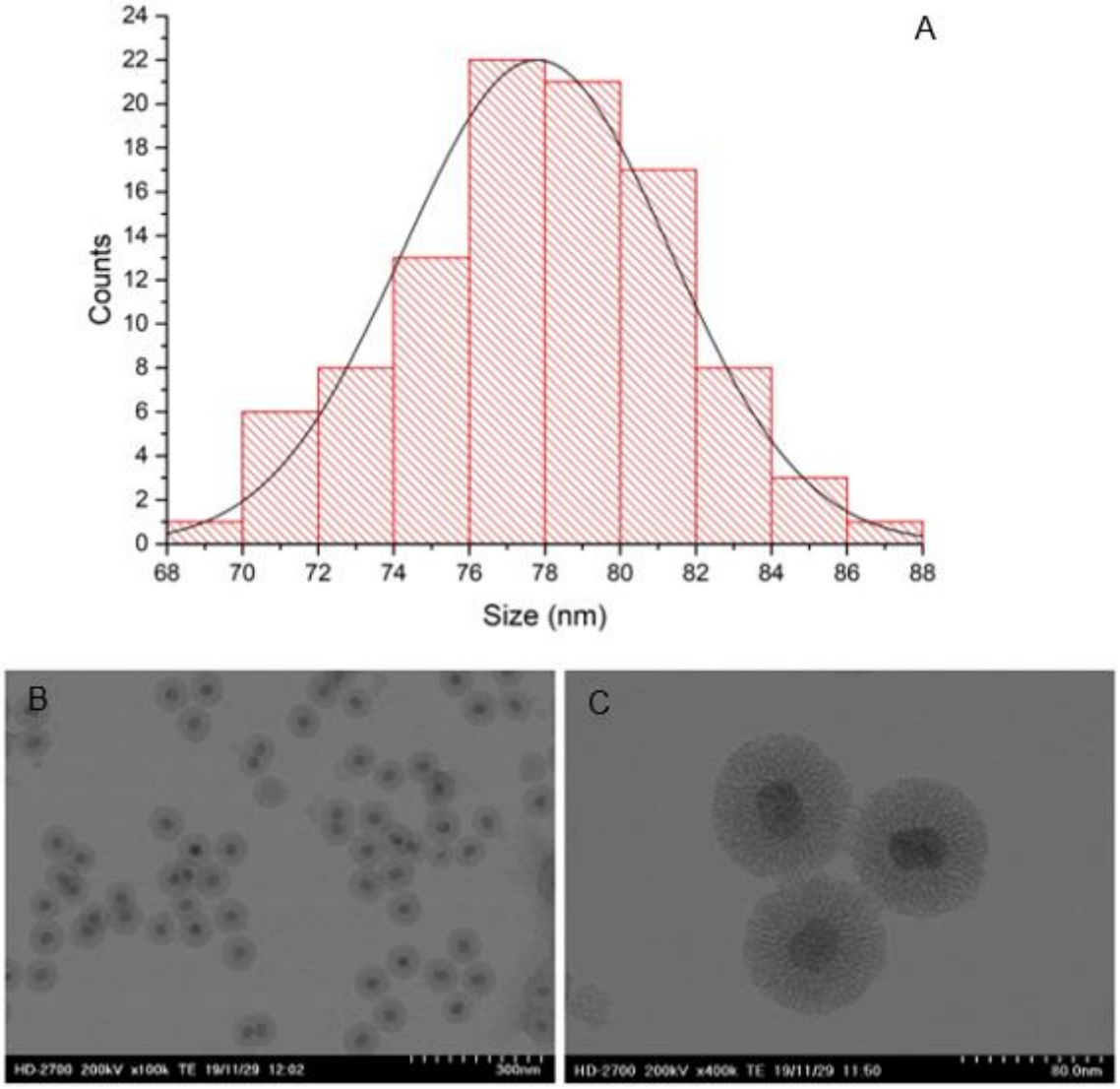

Figure 15: (A) Particle size distribution of $NaYF_4$UCNPs@$mSiO_2$ nanoparticles determined via image analysis with ImageJ, with an average nanoparticle size of 77.78 ± 3.53 nm. STEM images of $NaYF_4$@$mSiO_2$ nanoparticles at two different ampliations: (B) 100,000x and (C) 400,000x.

3.2 Cell viability

Cell viability was performed by WST-8 assay on 2 different nanoparticles: Gd_2O_3UCNPS, $NaYF_4$UCNPs@$mSiO_2$.

3.2.1 Gd_2O_3UCNPS

Gadolinium oxide UCNPs were tested on MNT-1 and A375 cell lines, for 24 and 48 hours (Figure 16).

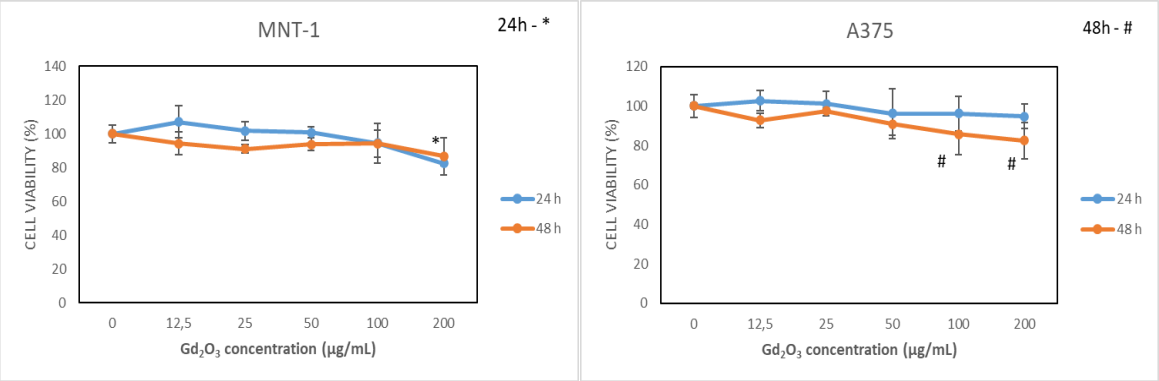

Figure 16: Cell viability by WST-8 protocol on MNT-1 (left) and A375 (right) cells, when exposed to Gd_2O_3 for 24 and 48 hours. Results are shown as average ± standard deviation (SD). * or # indicates significant statistical difference in relation to the control condition ($p<0.005$).

For all tested concentrations of Gd_2O_3UCNPS MNT-1 cell viability was above 90% with no statistical difference, showing that this nanoparticles do not affect the cell's viability. For A375 cells, viability 24 hours after exposure showed no statistical differences, but after 48 hours there was a significant decrease at 100 and 200 µg/mL, showing that these concentrations of nanoparticles result in a significant viability decrease.

3.2.2 $NaYF_4$UCNPs@$mSiO_2$

The nanoparticle $NaYF_4$UCNPs@$mSiO_2$ effect on viability was tested on 4 different cell lines: MNT-1, B16-F10, A375 and SK-MEL-28 (Figure 17).

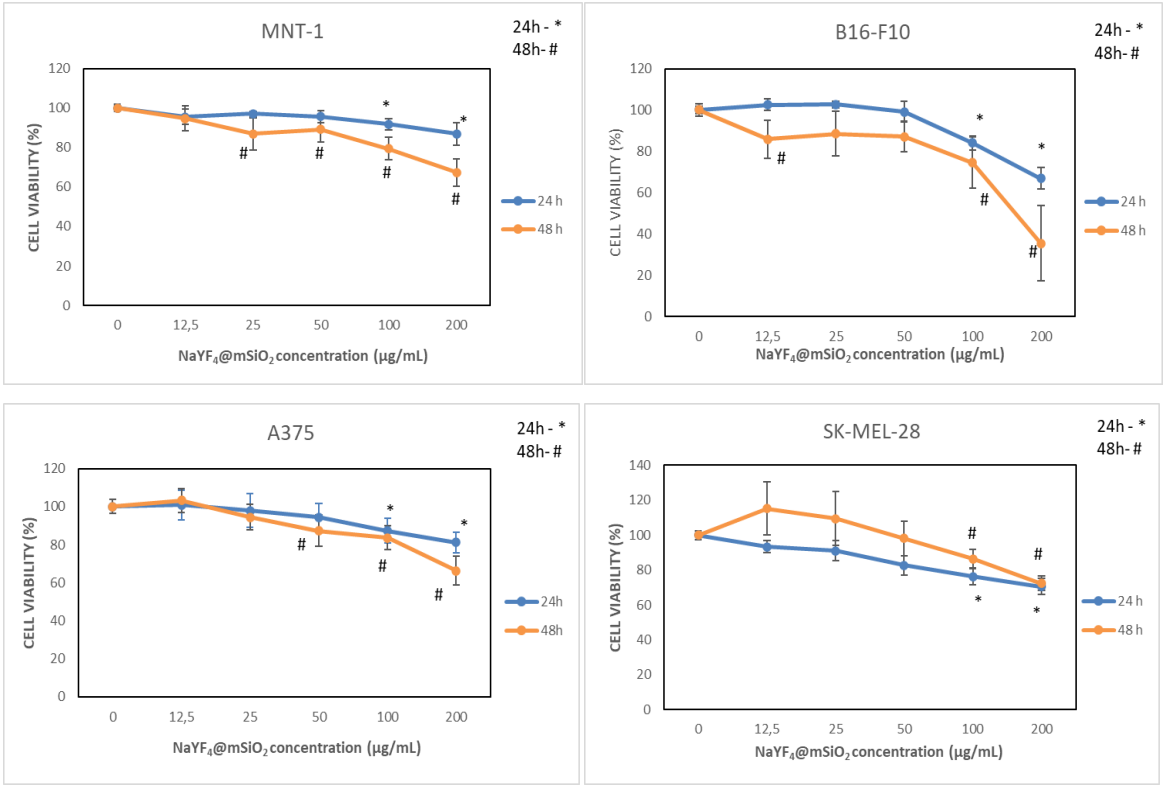

Figure 17: Cell viability by WST-8 protocol of MNT-1 (top left), B16-F10 (top right), A375 (bottom left) and SK-MEL-28 (bottom right) cells, when exposed to $NaYF_4$UCNPs@$mSiO_2$ for 24 and 48 hours. Results are shown as average ± standard deviation (SD). * or # indicates significant statistical difference in relation to the control condition ($p<0.005$).

On all cases there is a significant decrease in viability at 100 and 200 µg/mL of $NaYF_4$UCNPs@$mSiO_2$, implying that these concentrations are too high for further tests with these nanoparticles.

MNT-1 cells also showed that even a lower concentration of 25 µg/mL for 48 hours has a negative impact in cellular viability, suggesting either the use of low concentrations of nanoparticle for 48 hours exposure or a smaller exposure time. A375 cells show a similar profile as the MNT-1 cells, except that at 48 hours of exposure there was an only significant decrease in viability at 50 µg/mL and above.

3.3 Uptake

Uptake was measured by flow cytometry of the 4 cell lines used in this work, with $NaYF_4$UCNPs@$mSiO_2$ nanoparticles at 2 different concentrations, 25 and 100 µg/mL, and a control group that had no nanoparticles in the medium (Figure 18).

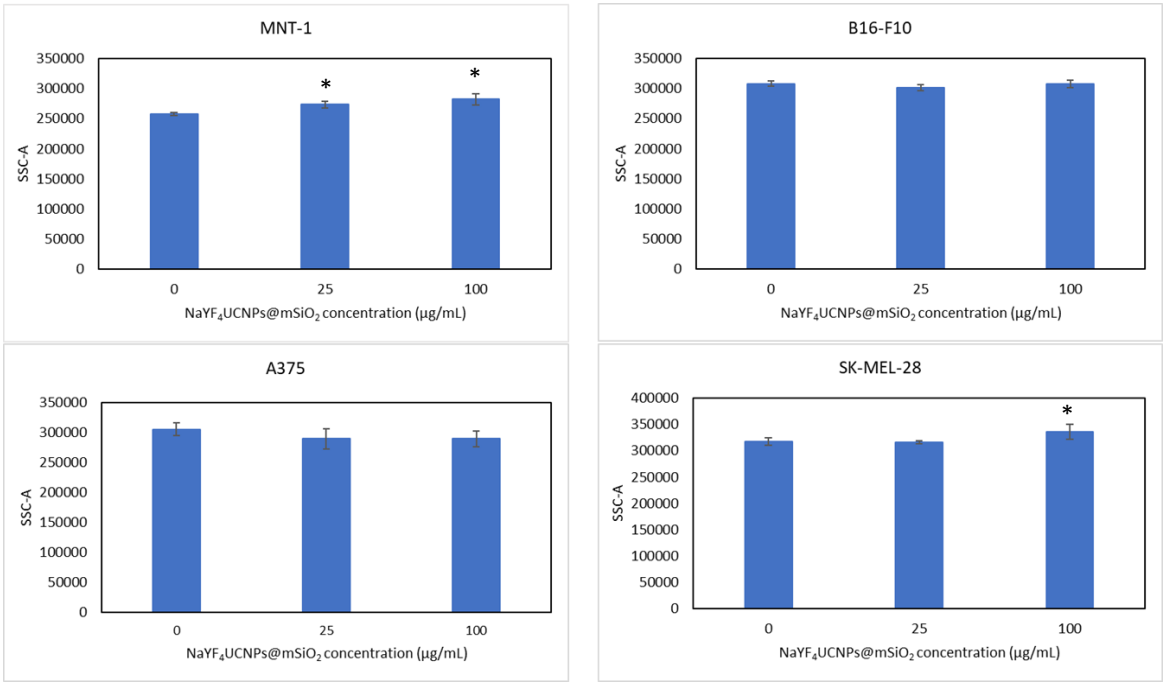

Figure 18: Cell uptake results of MNT-1 (top left), B16-F10 (top right), A375 (bottom left) and SK-MEL-28 (bottom right) cells, when exposed to 25 and 100 µg/mL of $NaYF_4UCNPs@mSiO_2$ for 24 hours. Results are shown as average ± standard deviation (SD). * indicates significant statistical difference in relation to the control condition ($p<0.005$).

The uptake results of SK-MEL-28 were transformed by square root to pass the normality test. This assay only showed a significant difference in MNT-1 cells that had more uptake when exposed to the nanoparticle in both concentrations, and SK-MEL-28, which only had a significant difference when exposed to 100 µg/mL.

3.4 Temperature exposure

The effects of heat on cells were measured by MTT cell viability assays after temperature exposure (Figure 19).

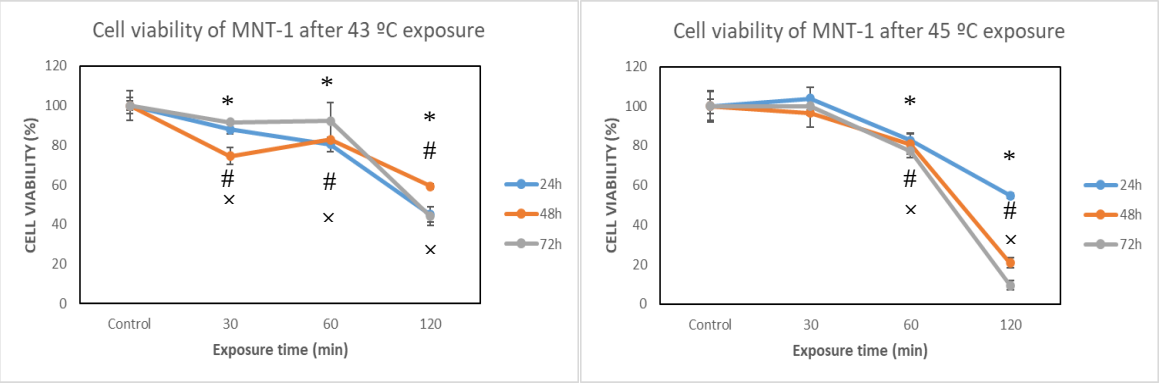

Figure 19: Cell viability by MTT protocol of MNT-1 cells when exposed to 43 ºC (left graph) and 45 ºC (right graph), for 30, 60, 90 and 120 minutes, 24 hours, 48 hours, and 72 hours after exposure. Results are shown as averages ± standard deviation (SD). * or # indicates significant statistical difference in relation to the control condition ($p<0.005$).

In these assays, we can see that a long exposure of temperature to MNT-1 cells causes lower cellular viability independently of how much time it has passed since the exposure, as shown by the low cellular viability of cells exposed for 120 minutes.

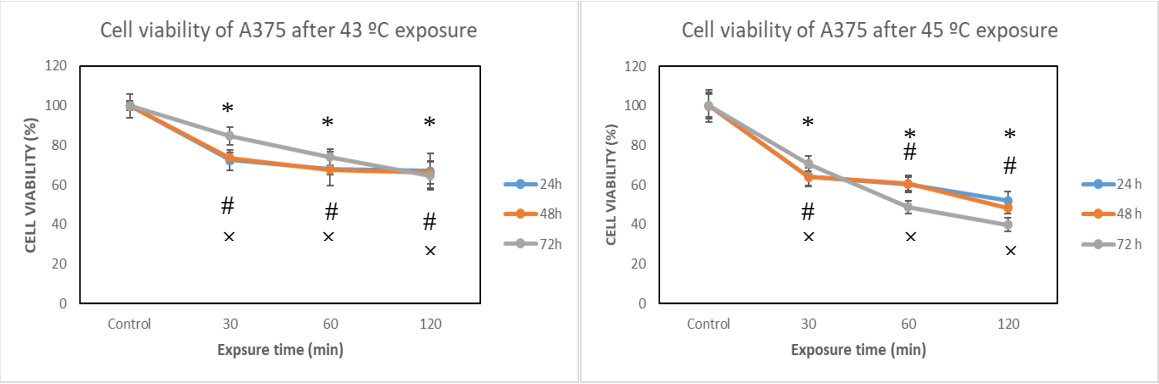

Figure 20: Cell viability by MTT protocol of A375 cells when exposed to 43 ºC (left graph) and 45 ºC (right graph), for 30, 60, 90 and 120 minutes, 24 hours, 48 hours, and 72 hours after exposure. Results are shown as averages ± standard deviation (SD). *, # or × indicates significant statistical difference in relation to the control condition ($p<0.005$).

A375 cells showed a uniform response in each temperature exposure, independently of the time of exposure. Cell viability, when exposed to 43 ºC, did not drop below 66%, while cell viability of cells exposed to 45 ºC showed lower results, with the lowest value of 39%, 72 hours after exposure for 120 minutes.

4. Discussion

This work assessed physicochemical properties of Gd_2O_3UCNPs and $NaYF_4$UCNPs@$mSiO_2$, and their dark cytotoxicity on melanoma cell lines. The effect of high temperature (43 and 45 ºC) on melanoma cell lines was also studied.

The physichochemical characterization of Gd_2O_3UCNPs showed overall high values of hydrodynamic diameter in both DMEM and dH_2O solutions, with dH_2O solution being the highest. Such high values can be the result of the agglomeration of these nanoparticles. This hypothesis is corroborated by the high PDI values, which shows high differences in size measurements of the nanoparticles. Furthermore, Zeta potential had values lower than -10 mV, which indicates the instability of the nanoparticles and tendency to aggregate [131]. These results show that the dispersion protocol used, ultrasonic bath for 20 minute, may not be appropriate to disperse correctly these nanoparticles.

$NaYF_4$UCNPs@$mSiO_2$ nanoparticles showed good values of hydrodynamic diameter in DMEM medium, while dH_2O medium had higher values in the tested concentrations, 25 and 100 µg/mL. Polydispersity index showed low values in dH_2O medium, which indicates that there was more uniformity in the sizes measured in the sample. On the other hand, DMEM medium values were higher, but this increase can be explained by the fact that this medium has different free-floating constituents, such as proteins, which increase the PDI reading. Zeta potential results showed that nanoparticles have electrostatic repulsion, but they were not fully stable [131]. Similar results concerning hydrodynamic diameter, PDI and Zeta potential, were obtained on similar nanoparticles, $NaYF_4$ nanoparticles, by Bazyńliska *et al.,* 2017 [132].

Scanning transmission electron microscopy showed that $NaYF_4$UCNPs@$mSiO_2$ had a size of 77.78 ± 3.53 nm, which are similar to the results reported by Li *et al.,* 2012 [133] in which $NaYF_4$UCNPs@$mSiO_2$ nanoparticles had a size around 80 nm. The hydrodynamic diameter of $NaYF_4$UCNPs@$mSiO_2$ nanoparticles was similar to the size determined by STEM at 25 µg/mL, with the hydrodynamic diameter at 100 µg/mL being slitly higher.

Cell viability assay of melanoma cells exposed to Gd_2O_3UCNPs showed a significant decrease of MNT-1 cells viability at 200 µg/mL at 24 hours after exposure.

A375 cells viability significantly decreased after exposure to 100 and 200 µg/mL during 48 hours. Even though there was a significant decrease in viability, it was maintained above 80% in all cases indicating a overall low cytotoxicity of Gd_2O_3UCNPs. Results obtained by *Li et al.,* 2015 reported a decrease in the viability of HeLa cells when exposed to Gd_2O_3UCNPs starting at a concentration of 281.25 µg/mL, but maintaining cell viability at 80% [134]. Even though the work conducted by *Li et.,* 2015 used higher concentrations of Gd_2O_3UCNPs the same overall profile can be seen, and this difference can be caused by different sensitivity of MNT-1 and A375 cells comparatively to HeLa cells [134].

Viability assays of $NaYF_4$UCNPs@$mSiO_2$ nanoparticles on the four melanoma cell lines were used to test the cytotoxicity of the nanoparticles, in order to discover at what concentration they can be used without harming the cells. In all four cell lines, there was no significant effect on the viability at 50 µg/mL, 24 hours after exposure. Hence, nanoparticles at this concentration can be used without causing a significantly negative effect on the cells. Results obtained by other studies with UCNPs applied on different cell lines also showed biocompatibility for concentrations at and below 50 µg/mL [135,136]. However, MNT-1 and A375 cells at 48 hours after exposure to 50 µg/mL of $NaYF_4$UCNPs@$mSiO_2$, showed a significant decrease in viability, with MNT-1 even showing a negative effect on viability with 25 µg/mL of $NaYF_4$UCNPs@$mSiO_2$. The results obtained demonstrate that for these two cell lines, the prolonged exposure to $NaYF_4$UCNPs@$mSiO_2$ at these concentrations has a negative impact on the viability.

Cell uptake assay was performed by flow cytometry, which compares the side scattering of the cells, indicating their granular complexity [137]. Based on this principle, a higher side scattering indicates the presence of nanoparticles inside the cell [137]. The results showed a significant increase of MNT-1 cells side scatter after exposure to both UCNPs concentrations used (25 and 100 µg/mL). SK-MEL-28 cells increased the side scatter only after exposure to the highest concentration, while A375 and B16-F10 cells did not show any differences. Even though uptake by flow cytometry is not as reliable as microscopic techniques, it serves as a preliminary result, indicating that at least MNT-1 and B16-F10 cells are able to uptake $NaYF_4$UCNPs@$mSiO_2$. The uptake of nanoparticles might be restricted if a negative

charge is present on the surface of the nanoparticles, which can cause an electrostatic repulsion with the cell membrane [138–140]. Cellular uptake of UCNPs might be increased by modifications of the surface, for example by adding folic acid or poly(ethylene glycol), as reported in several studies [100,109].

Temperature assays showed that hyperthermia causes cellular death in a time and temperature-dependent manner, with cell viability of MNT-1 cells being lower within higher exposure time and temperature (120 min at 45 ºC). MNT-1 cells exposed to 43 ºC showed similar viability responses, independently of the time after exposure. Such might be explained by the fact that temperature of 43 ºC causes reversible cellular damage [141], and that the cells 24 hours after exposure did not have enough time to revert the damages, showing similar cell viability as the cells exposed to 45 ºC. MNT-1 cells when exposed to 45 ºC showed a similar profile of response, with the only difference being on the exposure time of 120 minutes, where 24 hours after exposure present a higher viability than the other two cases. This might be explained by the fact that cells were still in the process of cell death, and as such 24 hours after exposure there was a higher viability than 48 and 72 hours after exposure. Similar results were obtained in other studies, such as Shellman *et al.* 2008 [56] which reported a decrease in cell viability of A375 cells when exposed to 45 ºC. A375 cells exposed to 43 ºC showed a similar pattern of cell viability, independently of how much time it had passed since the exposure, with cell viability not dropping below 60% in all cases. Similar results were reported by Shellman *et al.* 2008 [56], in which viability of A375 cells dropped to around 40% when exposed to 45 ºC, but it did not suffer alterations when exposed to 41 ºC, and as such, the temperature of 43 ºC yielded results in between the two temperatures reported. The same A375 cells when exposed to 45 ºC showed lower cell viability, as expected, with cell viability 24 and 48 hours after exposure showing similar results, never dropping below 50%. However, cell viability 72 hours after exposure had lower cell viability in every period tested, with the lowest being 39% at 120 minutes of exposure. Cell viability results 24 hours after exposure, showed lower viability at 30 and 60 minutes exposure than the results reported by Shellman *et al.* 2008 [56], but the viability after 90 minutes was around 40%, however in this work showed the same viability at 120 min. Even though there are differences between the results

obtained in this work and Shellman *et al.* 2008 [56], they share a similar profile, and these differences can be explained by the different effect hyperthermia has on the same cells in different phases for the cell cycle [49].

Even though the mechanism of cell death was not explored in this thesis, several studies have shown that it mostly happens by apoptosis at a temperature of 43 ºC [56,142], and necrosis with higher temperature, such as 45 ºC [49,143].

5. Final remarks

Cancer is one of the most common diseases and one with a higher mortality rate, and as such, there is a need to create new approaches to treat it. Hyperthermia has long been studied as a therapeutic treatment for cancer since heat affects the biochemical process of the tumour cells leading to their death. However, this therapeutic technique has its limitations, such as the inability to apply heat only to tumour cells.

Nanoparticles have been revolutionary in the sciences, and their use spreads throughout all branches. Many advances have been made in this area, and in present times upconversion nanoparticles have garnered a lot of interest for their special characteristics, such as their anti-stokes shift. These nanoparticles, have been applied to generate hyperthermia. They offer the ability to provoke hyperthermia from the inside-out and to target cancer cells with the possibility of all this being done noninvasively by lasers.

In this work, we established a range of concentrations of $NaYF_4$@$mSiO_2$ that is possible to use without affecting the viability of the four different cell lines used, and also a range of concentration of Gd_2O_3UCNPS for MNT-1 and A375 cell lines. The aim of this work was also to study the response profile of melanoma cell lines to hyperthermia which was obtained for MNT-1 and A375 cell lines after exposure to 43 ºC and 45 ºC for different times. In this study it was possible to see that viability drops with time of exposure, and that higher temperatures induced lower viability.

The conditions defined in the current work (UCNPs concentrations and temperatures) can be replicated in the future in order to generate near-infrared light triggered hyperthermia in melanoma cells using UCNPs.

6. References

1. *Health at a Glance: Europe 2018 (Summary in Spanish)*.; 2018. doi:10.1787/fd41e65f-es
2. WHO n.d. Cancer today. WHO n.d. http://gco.iarc.fr/today/home (accessed June 15, 2020).
3. Olaku OO, Taylor EA. Cancer in the Medically Underserved Population. *Physician Assist Clin*. 2019;4(1):275-285. doi:10.1016/j.cpha.2018.08.011
4. Silva A. Assessment of antitumor and antibacterial potential of Vipera latastei venom. Published online 2019.
5. Hanahan D, Weinberg RA. Hallmarks of cancer: The next generation. *Cell*. 2011;144(5):646-674. doi:10.1016/j.cell.2011.02.013
6. Carr S, Smith C, Wernberg J. Epidemiology and Risk Factors of Melanoma. *Surg Clin North Am*. 2020;100(1):1-12. doi:10.1016/j.suc.2019.09.005
7. Cancer Facts and Figures, Statistics for 2008, Facts sheets, Skin Cancer.
8. østerlind A. Epidemiology on malignant melanoma in europe. *Acta Oncol (Madr)*. 1992;31(8):903-908. doi:10.3109/02841869209089727
9. Albert VA, Koh HK, Geller AC, Miller DR, Prout MN, Lew RA. Years of potential life lost: Another indicator of the impact of cutaneous malignant melanoma on society. *J Am Acad Dermatol*. 1990;23(2):308-310. doi:10.1016/0190-9622(90)70214-3
10. Wong VK, Lubner MG, Menias CO, et al. Clinical and imaging features of noncutaneous melanoma. *Am J Roentgenol*. 2017;208(5):943-959. doi:10.2214/AJR.16.16800
11. Caini S, Gandini S, Sera F, et al. Meta-analysis of risk factors for cutaneous melanoma according to anatomical site and clinico-pathological variant. *Eur J Cancer*. 2009;45(17):3054-3063. doi:10.1016/j.ejca.2009.05.009
12. Melanoma Risk Factor. *Definitions*. 2020;1012:1005-1011. doi:10.32388/7xj0gw
13. Green A, Autier P, Boniol M, et al. The association of use of sunbeds with cutaneous malignant melanoma and other skin cancers: A systematic review. *Int J Cancer*. 2007;120(5):1116-1122. doi:10.1002/ijc.22453

14. Rünger TM. C→T transition mutations are not solely UVB-signature mutations, because they are also generated by UVA. *J Invest Dermatol*. 2008;128(9):2138-2140. doi:10.1038/jid.2008.165
15. Pattison DI, Davies MJ. Actions of ultraviolet light on cellular structures. *EXS*. 2006;(96):131-157. doi:10.1007/3-7643-7378-4_6
16. Dakup P, Gaddameedhi S. Impact of the Circadian Clock on UV-Induced DNA Damage Response and Photocarcinogenesis. *Photochem Photobiol*. 2017;93(1):296-303. doi:10.1111/php.12662
17. Troy T, Jekic-McMullen D, Sambucetti L, Rice B. Quantitative comparison of the sensitivity of detection of fluorescent and bioluminescent reporters in animal models. *Mol Imaging*. 2004;3(1):9-23. doi:10.1162/153535004773861688
18. Kangasniemi M, McNichols RJ, Bankson JA, Gowda A, Price RE, Hazle JD. Thermal therapy of canine cerebral tumors using a 980 nm diode laser with MR temperature-sensitive imaging feedback. *Lasers Surg Med*. 2004;35(1):41-50. doi:10.1002/lsm.20069
19. Idris NM, Jayakumar MKG, Bansal A, Zhang Y. Upconversion nanoparticles as versatile light nanotransducers for photoactivation applications. *Chem Soc Rev*. 2015;44(6):1449-1478. doi:10.1039/c4cs00158c
20. Nishigori C, Yarosh DB, Ullrich SE, et al. Evidence that DNA damage triggers interleukin 10 cytokine production in UV-irradiated murine keratinocytes. *Proc Natl Acad Sci U S A*. 1996;93(19):10354-10359. doi:10.1073/pnas.93.19.10354
21. Kunisada M, Yogianti F, Sakumi K, Ono R, Nakabeppu Y, Nishigori C. Increased expression of versican in the inflammatory response to UVB- and reactive oxygen species-induced skin tumorigenesis. *Am J Pathol*. 2011;179(6):3056-3065. doi:10.1016/j.ajpath.2011.08.042
22. Afaq F, K. Katiyar S. Polyphenols: Skin Photoprotection and Inhibition of Photocarcinogenesis. *Mini-Reviews Med Chem*. 2012;11(14):1200-1215. doi:10.2174/13895575111091200
23. Bevona C, Goggins W, Quinn T, Fullerton J, Tsao H, Corona R. Cutaneous Melanomas Associated with Nevi. *Arch Dermatol*. 2003;139(12):1620-1624.

doi:10.1001/archderm.139.12.1620

24. Ford D, Bliss JM, Swerdlow AJ, et al. Risk of cutaneous melanoma associated with a family history of the disease. *Int J Cancer*. 1995;62(4):377-381. doi:10.1002/ijc.2910620403
25. Gandini S, Sera F, Cattaruzza MS, et al. Meta-analysis of risk factors for cutaneous melanoma: I. Common and atypical naevi. *Eur J Cancer*. 2005;41(1):28-44. doi:10.1016/j.ejca.2004.10.015
26. Halpern AC, Iv DG, Elder DE, et al. Dysplastic Nevi as Risk Markers of Sporadic (Nonfamilial) Melanoma. Published online 2015:4-8.
27. Shain AH, Yeh I, Kovalyshyn I, et al. The genetic evolution of melanoma from precursor lesions. *N Engl J Med*. 2015;373(20):1926-1936. doi:10.1056/NEJMoa1502583
28. Kittler H, Pehamberger H, Wolff K, Binder M. Diagnostic accuracy of dermoscopy. *Lancet Oncol*. 2002;3(3):159-165. doi:10.1016/S1470-2045(02)00679-4
29. Larkin J, Chiarion-Sileni V, Gonzalez R, et al. Combined nivolumab and ipilimumab or monotherapy in untreated Melanoma. *N Engl J Med*. 2015;373(1):23-34. doi:10.1056/NEJMoa1504030
30. De Velasco G, Je Y, Bossé D, et al. Comprehensive meta-analysis of key immune-related adverse events from CTLA-4 and PD-1/PD-L1 inhibitors in cancer patients. *Cancer Immunol Res*. 2017;5(4):312-318. doi:10.1158/2326-6066.CIR-16-0237
31. Kaufman HL, Ruby CE, Hughes T, Slingluff CL. Current status of granulocyte-macrophage colony-stimulating factor in the immunotherapy of melanoma. *J Immunother Cancer*. 2014;2(1). doi:10.1186/2051-1426-2-11
32. Ballantyne AD, Garnock-Jones KP. Dabrafenib: First global approval. *Drugs*. 2013;73(12):1367-1376. doi:10.1007/s40265-013-0095-2
33. Hertzman Johansson C, Egyhazi Brage S. BRAF inhibitors in cancer therapy. *Pharmacol Ther*. 2014;142(2):176-182. doi:10.1016/j.pharmthera.2013.11.011
34. Hauschild A, Grob JJ, Demidov L V, et al. Dabrafenib in BRAF-mutated metastatic melanoma: A multicentre, open-label, phase 3 randomised

controlled trial. *Lancet*. 2012;380(9839):358-365. doi:10.1016/S0140-6736(12)60868-X

35. Dickson P V, Gershenwald JE. Staging and prognosis of cutaneous melanoma. *Surg Oncol Clin N Am*. 2011;20(1):1-17. doi:10.1016/j.soc.2010.09.007
36. Pardoll DM. The blockade of immune checkpoints in cancer immunotherapy. *Nat Rev Cancer*. 2012;12(4):252-264. doi:10.1038/nrc3239
37. Baronzio G, Parmar G, Ballerini M, Szasz A. A Brief Overview of Hyperthermia in Cancer Treatment. *J Integr Oncol*. 2014;03(01). doi:10.4172/2329-6771.1000115
38. W B. Uber den Einfluss welche heftigere Erysipeln zuweilig auf organisierte Neubildungenausuben. *Verhandlungen des Naturhistorischen Vereines der Preuss Rheinlande undWestphalens*. 1866;23:28-30.
39. P B. Die heilwirkung des erysipels auf geschwulste. *Beitr Klin Chir*. 1887;3:443-446.
40. Coley WB. I. The Treatment of Malignant Tumors by Repeated Inoculations of Erysipelas. *Ann Surg*. 1893;18:68. doi:10.1097/00000658-189307000-00009
41. Pontiggia P, McLaren J, Baronzio G. The biological responses to heat. *Adv Exp Med Biol*. 1990;267(6):271-291. doi:10.1007/978-1-4684-5766-7_4
42. Pietrangeli P, Mondovì B. On the Biochemical Basis of Tumour Damage by Hypothermia. In: *Hyperthermia in Cancer Treatment: A Primer*. Springer US; 2006:110-118. doi:10.1007/978-0-387-33441-7_8
43. Cui ZG, Piao JL, Rehman MUR, et al. Molecular mechanisms of hyperthermia-induced apoptosis enhanced by withaferin A. *Eur J Pharmacol*. 2014;723(1):99-107. doi:10.1016/j.ejphar.2013.11.031
44. Szasz O, Andocs G, Meggyeshazi N. Oncothermia as Personalized Treatment Option. *Conf Pap Med*. 2013;2013:1-6. doi:10.1155/2013/941364
45. Koutcher JA, Barnett D, Kornblith AB, Cowburn D, Brady TJ, Gerweck LE. Relationship of changes in pH and energy status to hypoxic cell fraction and hyperthermia sensitivity. *Int J Radiat Oncol Biol Phys*. 1990;18(6):1429-1435. doi:10.1016/0360-3016(90)90318-E

46. Gerweck LE, Seetharaman K. Cellular pH gradient in tumor versus normal tissue: Potential exploitation for the treatment of cancer. *Cancer Res*. 1996;56(6):1194-1198.
47. Baronzio G, Cerreta V, Baronzio A, Freitas I, Mapelli M, Gramaglia A. Thermo-Chemo-Radiotherapy Association: Biological Rationale, Preliminary Observations on Its Use on Malignant Brain Tumors. *Madame Curie Biosci Database [Internet]*. Published online 2013.
48. Hahn GM. Metabolic Aspects of the Role of Hyperthermia in Mammalian Cell Inactivation and Their Possible Relevance to Cancer Treatment. *Cancer Res*. 1974;34(11):3117-3123.
49. Hildebrandt B, Wust P, Ahlers O, et al. The cellular and molecular basis of hyperthermia. *Crit Rev Oncol Hematol*. 2002;43(1):33-56. doi:10.1016/S1040-8428(01)00179-2
50. Yoshihisa Sakaguchi L, Stephens C, Makino M, et al. Apoptosis in Tumors and Normal Tissues Induced by Whole Body Hyperthermia in Rats. Published online 1995.
51. Coss RA, Dewey C, Bamburg JR. Effects of Hyperthermiaon DividingChinese HamsterOvary Cells and on Microtubulesin Vitro1. 1982;(MARCH).
52. Dewey WC. The Search for Critical Cellular Targets Damaged by Heat. *Radiat Res*. 1989;120(2):191-204. http://www.ncbi.nlm.nih.gov/pubmed/2694212
53. Ahmed K, Zaidi SF. Treating cancer with heat: Hyperthermia as promising strategy to enhance apoptosis. *J Pak Med Assoc*. 2013;63(4):504-508.
54. Ahmed K, Zaidi SF. Hyperthermia Chemo-sensitization, Chemical Thermo-sensitization and Apoptosis. 2013;63(4):504-508.
55. Liang H, Zhan HJ, Wang BG, Pan Y, Hao XS. Change in expression of apoptosis genes after hyperthermia, chemotherapy and radiotherapy in human colon cancer transplanted into nude mice. *World J Gastroenterol*. 2007;13(32):4365-4371. doi:10.3748/wjg.v13.i32.4365
56. Shellman YG, Howe WR, Miller LA, et al. Hyperthermia induces endoplasmic reticulum-mediated apoptosis in melanoma and non-melanoma

skin cancer cells. *J Invest Dermatol*. 2008;128(4):949-956. doi:10.1038/sj.jid.5701114

57. Meniawy TM, Nowak AK, Lake RA. Effect of Chemotherapy on the Tumor Microenvironment and Anti-tumor Immunity. In: *Tumor Ablation*. Springer Netherlands; 2013:1-28. doi:10.1007/978-94-007-4694-7_1
58. Lee CT, MacE T, Repasky EA. Hypoxia-driven immunosuppression: A new reason to use thermal therapy in the treatment of cancer? *Int J Hyperth*. 2010;26(3):232-246. doi:10.3109/02656731003601745
59. Baronzio G, Gramaglia A, Fiorentini G. Hyperthermia and immunity. A brief overview. *In Vivo (Brooklyn)*. 2006;20(6 A):689-696.
60. Mondovi B, Santoro AS, Strom R, Faiola R, Fanelli AR. INCREASED IMMUNOGENICITY OF EHRLICH ASCITES CELLS AFTER HEAT TREATMENT. *Appl Biochem*. Published online 1982:885-888.
61. Roca C, Primo L, Valdembri D, et al. Hyperthermia inhibits angiogenesis by a plasminogen activator inhibitor 1-dependent mechanism. *Cancer Res*. 2003;63(7):1500-1507.
62. Habash RWY, Bansal R, Krewski D, Alhafid HT. Thermal therapy, Part 2: Hyperthermia techniques. *Crit Rev Biomed Eng*. 2006;34(6):491-542. doi:10.1615/CritRevBiomedEng.v34.i6.30
63. Vernon CC, van der Zee J. Hyperthermia in cancer treatment. *Lancet*. 1995;345(8965):1-48.
64. Kaur P, Aliru ML, Chadha AS, Asea A, Krishnan S. Hyperthermia using nanoparticles - Promises and pitfalls. *Int J Hyperth*. 2016;32(1):76-88. doi:10.3109/02656736.2015.1120889
65. Laurent S, Forge D, Port M, et al. Magnetic iron oxide nanoparticles: Synthesis, stabilization, vectorization, physicochemical characterizations and biological applications. *Chem Rev*. 2008;108(6):2064-2110. doi:10.1021/cr068445e
66. Shin WK, Cho J, Kannan AG, Lee YS, Kim DW. Cross-linked Composite Gel Polymer Electrolyte using Mesoporous Methacrylate-Functionalized SiO2 Nanoparticles for Lithium-Ion Polymer Batteries. *Sci Rep*. 2016;6(April):1-10. doi:10.1038/srep26332

67. Bakand S, Hayes A. Toxicological considerations, toxicity assessment, and risk management of inhaled nanoparticles. *Int J Mol Sci*. 2016;17(6):1-17. doi:10.3390/ijms17060929
68. Fariq A, Khan T, Yasmin A. Microbial synthesis of nanoparticles and their potential applications in biomedicine. *J Appl Biomed*. 2017;15(4):241-248. doi:10.1016/j.jab.2017.03.004
69. Jørgensen CK. Lanthanides since 1839: From crowded elements to quantum-chemical Rosetta Stone. *Inorganica Chim Acta*. 1987;139(1-2):1-5. doi:10.1016/S0020-1693(00)84026-8
70. Eliseeva S V, Bünzli JCG. Rare earths: Jewels for functional materials of the future. *New J Chem*. 2011;35(6):1165-1176. doi:10.1039/c0nj00969e
71. Bethencourt M, Botana FJ, Calvino JJ, Marcos M, RodrÍguez-Chacón MA. Lanthanide compounds as environmentally-friendly corrosion inhibitors of aluminium alloys: a review. *Corros Sci*. 1998;40(11):1803-1819. doi:10.1016/S0010-938X(98)00077-8
72. Gonzalez V, Vignati DAL, Leyval C, Giamberini L. Environmental fate and ecotoxicity of lanthanides: Are they a uniform group beyond chemistry? *Environ Int*. 2014;71:148-157. doi:10.1016/j.envint.2014.06.019
73. Lin M, Zhao Y, Wang SQ, et al. Recent advances in synthesis and surface modification of lanthanide-doped upconversion nanoparticles for biomedical applications. *Biotechnol Adv*. 2012;30(6):1551-1561. doi:10.1016/j.biotechadv.2012.04.009
74. Huang Y, Sun S, Friscic T, Forgione P. Upconverting Nanoparticles for Integration in. Published online 2017.
75. Auzel F. Upconversion and Anti-Stokes Processes with f and d Ions in Solids. *Chem Rev*. 2004;104(1):139-173. doi:10.1021/cr020357g
76. Heffern MC, Matosziuk LM, Meade TJ. Lanthanide probes for bioresponsive imaging. *Chem Rev*. 2014;114(8):4496-4539. doi:10.1021/cr400477t
77. Chen G, Qiu H, Prasad PN, Chen X. Upconversion nanoparticles: Design, nanochemistry, and applications in Theranostics. *Chem Rev*. 2014;114(10):5161-5214. doi:10.1021/cr400425h
78. Renero-Lecuna C, Martín-Rodríguez R, Valiente R, et al. Origin of the high

upconversion green luminescence efficiency in $β$-NaYF4:2%Er3+,20%Yb3+. *Chem Mater*. 2011;23(15):3442-3448. doi:10.1021/cm2004227

79. Kumar R, Nyk M, Ohulchanskyy TY, Flask CA, Prasad PN. Combined optical and MR bloimaging using rare earth ion doped NaYF 4 nanocrystals. *Adv Funct Mater*. 2009;19(6):853-859. doi:10.1002/adfm.200800765
80. Chen G, Ohulchanskyy TY, Kumar R, Ågren H, Prasad PN. Ultrasmall monodisperse NaYF4:Yb3+/Tm3+ nanocrystals with enhanced near-infrared to near-infrared upconversion photoluminescence. *ACS Nano*. 2010;4(6):3163-3168. doi:10.1021/nn100457j
81. Yi GS, Chow GM. Synthesis of hexagonal-phase NaYF4:Yb,Er and NaYF 4:Yb,Tm nanocrystals with efficient up-conversion fluorescence. *Adv Funct Mater*. 2006;16(18):2324-2329. doi:10.1002/adfm.200600053
82. Boyer JC, Cuccia LA, Capobianco JA. Synthesis of colloidal upconverting NaYF4: Er3+/Yb3+ and Tm3+/Yb3+ monodisperse nanocrystals. *Nano Lett*. 2007;7(3):847-852. doi:10.1021/nl070235+
83. Vetrone F, Naccache R, Mahalingam V, Morgan CG, Capobianco JA. The active-core/active-shell approach: A strategy to enhance the upconversion luminescence in lanthanide-doped nanoparticles. *Adv Funct Mater*. 2009;19(18):2924-2929. doi:10.1002/adfm.200900234
84. Naccache R, Vetrone F, Mahalingam V, Cuccia LA, Capobianco JA. Controlled synthesis and water dispersibility of hexagonal phase NaGdF 4:Ho3+/Yb3+ nanoparticles. *Chem Mater*. 2009;21(4):717-723. doi:10.1021/cm803151y
85. Liu Q, Sun Y, Yang T, Feng W, Li C, Li F. Sub-10 nm hexagonal lanthanide-doped NaLuF 4 upconversion nanocrystals for sensitive bioimaging in vivo. *J Am Chem Soc*. 2011;133(43):17122-17125. doi:10.1021/ja207078s
86. Krämer KW, Biner D, Frei G, Güdel HU, Hehlen MP, Lüthi SR. Hexagonal Sodium Yttrium Fluoride Based Green and Blue Emitting Upconversion Phosphors. *Chem Mater*. 2004;16(7):1244-1251. doi:10.1021/cm031124o
87. Wang F, Liu X. Recent advances in the chemistry of lanthanide-doped upconversion nanocrystals. *Chem Soc Rev*. 2009;38(4):976-989.

doi:10.1039/b809132n

88. Quintanilla M, Ren F, Ma D, Vetrone F. Light Management in Upconverting Nanoparticles: Ultrasmall Core/Shell Architectures to Tune the Emission Color. *ACS Photonics*. 2014;1(8):662-669. doi:10.1021/ph500208q
89. Wang H, Nann T. Monodisperse upconversion GdF3:Yb, Er rhombi by microwave-assisted synthesis. *Nanoscale Res Lett*. 2011;6(1):3-7. doi:10.1186/1556-276X-6-267
90. Wang Y, Cai R, Liu Z. Controlled synthesis of NaYF4: Yb, Er nanocrystals with upconversion fluorescence via a facile hydrothermal procedure in aqueous solution. *CrystEngComm*. 2011;13(6):1772-1774. doi:10.1039/c0ce00708k
91. Zhang Q, Yan B. Phase control of upconversion nanocrystals and new rare earth fluorides though a diffusion-controlled strategy in a hydrothermal system. *Chem Commun*. 2011;47(20):5867-5869. doi:10.1039/c1cc11367d
92. Boyer JC, Vetrone F, Cuccia LA, Capobianco JA. Synthesis of colloidal upconverting NaYF4 nanocrystals doped with Er3+, Yb3+ and Tm3+, Yb3+ via thermal decomposition of lanthanide trifluoroacetate precursors. *J Am Chem Soc*. 2006;128(23):7444-7445. doi:10.1021/ja061848b
93. Mai HX, Zhang YW, Si R, et al. High-quality sodium rare-earth fluoride nanocrystals: Controlled synthesis and optical properties. *J Am Chem Soc*. 2006;128(19):6426-6436. doi:10.1021/ja060212h
94. Zhang YW, Sun X, Si R, You LP, Yan CH. Single-crystalline and monodisperse LaF3 triangular nanoplates from a single-source precursor. *J Am Chem Soc*. 2005;127(10):3260-3261. doi:10.1021/ja042801y
95. Wu AM, Gambhir SS, Weiss S. Quantum Dots for Live Cetis ,. *Science (80-)*. 2016;307(5709):538-544.
96. Resch-Genger U, Grabolle M, Cavaliere-Jaricot S, Nitschke R, Nann T. Quantum dots versus organic dyes as fluorescent labels. *Nat Methods*. 2008;5(9):763-775. doi:10.1038/nmeth.1248
97. Zhou J, Liu Z, Li F. Upconversion nanophosphors for small-animal imaging. *Chem Soc Rev*. 2012;41(3):1323-1349. doi:10.1039/c1cs15187h
98. Wang M, Abbineni G, Clevenger A, Mao C, Xu S. Upconversion

nanoparticles: Synthesis, surface modification and biological applications. *Nanomedicine Nanotechnology, Biol Med*. 2011;7(6):710-729. doi:10.1016/j.nano.2011.02.013

99. Ang LY, Lim ME, Ong LC, Zhang Y. Applications of upconversion nanoparticles in imaging, detection and therapy. *Nanomedicine*. 2011;6(7):1273-1288. doi:10.2217/nnm.11.108
100. Boyer JC, Manseau MP, Murray JI, Van Veggel FCJM. Surface modification of upconverting NaYF4 nanoparticles with PEG-phosphate ligands for NIR (800 nm) biolabeling within the biological window. *Langmuir*. 2010;26(2):1157-1164. doi:10.1021/la902260j
101. Cao T, Yang Y, Gao Y, Zhou J, Li Z, Li F. High-quality water-soluble and surface-functionalized upconversion nanocrystals as luminescent probes for bioimaging. *Biomaterials*. 2011;32(11):2959-2968. doi:10.1016/j.biomaterials.2010.12.050
102. Chen J, Guo C, Wang M, et al. Controllable synthesis of NaYF4:Yb,Er upconversion nanophosphors and their application to in vivo imaging of Caenorhabditis elegans. *J Mater Chem*. 2011;21(8):2632-2638. doi:10.1039/c0jm02854a
103. Sun Y, Yu M, Liang S, et al. Fluorine-18 labeled rare-earth nanoparticles for positron emission tomography (PET) imaging of sentinel lymph node. *Biomaterials*. 2011;32(11):2999-3007. doi:10.1016/j.biomaterials.2011.01.011
104. Liu H, Xu CT, Andersson-Engels S. Multibeam fluorescence diffuse optical tomography using upconverting nanoparticles. *Opt Lett*. 2010;35(5):718. doi:10.1364/ol.35.000718
105. Qian HS, Guo HC, Ho PCL, Mahendran R, Zhang Y. Mesoporous-silica-coated up-conversion fluorescent nanoparticles for photodynamic therapy. *Small*. 2009;5(20):2285-2290. doi:10.1002/smll.200900692
106. Idris NM, Gnanasammandhan MK, Zhang J, Ho PC, Mahendran R, Zhang Y. In vivo photodynamic therapy using upconversion nanoparticles as remote-controlled nanotransducers. *Nat Med*. 2012;18(10):1580-1585. doi:10.1038/nm.2933

107. Wang C, Cheng L, Liu Z. Drug delivery with upconversion nanoparticles for multi-functional targeted cancer cell imaging and therapy. *Biomaterials*. 2011;32(4):1110-1120. doi:10.1016/j.biomaterials.2010.09.069
108. Liu J, Bu W, Pan L, Shi J. NIR-triggered anticancer drug delivery by upconverting nanoparticles with integrated azobenzene-modified mesoporous silica. *Angew Chemie - Int Ed*. 2013;52(16):4375-4379. doi:10.1002/anie.201300183
109. Lai J, Shah BP, Zhang Y, Yang L, Lee KB. Real-time monitoring of ATP-responsive drug release using mesoporous-silica-coated multicolor upconversion nanoparticles. *ACS Nano*. 2015;9(5):5234-5245. doi:10.1021/acsnano.5b00641
110. Cheng L, Yang K, Li Y, et al. Facile preparation of multifunctional upconversion nanoprobes for multimodal imaging and dual-targeted photothermal therapy. *Angew Chemie - Int Ed*. 2011;50(32):7385-7390. doi:10.1002/anie.201101447
111. Huang Y, Rosei F, Vetrone F. A single multifunctional nanoplatform based on upconversion luminescence and gold nanorods. *Nanoscale*. 2015;7(12):5178-5185. doi:10.1039/C4NR07369J
112. Vetrone F, Naccache R, Capobianco JA, Juarranz A, Rodriguez EM, Jaque D. Electronic Supplementary Information Intracellular imaging of HeLa cells by non-functionalized. 2009;(c):1-4.
113. Shan J, Chen J, Meng J, et al. Biofunctionalization, cytotoxicity, and cell uptake of lanthanide doped hydrophobically ligated NaYF4 upconversion nanophosphors. *J Appl Phys*. 2008;104(9):1-7. doi:10.1063/1.3008028
114. Lim SF, Riehn R, Ryu WS, et al. In vivo and scanning electron microscopy imaging of upconverting nanophosphors in Caenorhabditis elegans. *Nano Lett*. 2006;6(2):169-174. doi:10.1021/nl0519175
115. Chatterjee DK, Rufaihah AJ, Zhang Y. Upconversion fluorescence imaging of cells and small animals using lanthanide doped nanocrystals. *Biomaterials*. 2008;29(7):937-943. doi:10.1016/j.biomaterials.2007.10.051
116. Xing H, Bu W, Zhang S, et al. Multifunctional nanoprobes for upconversion fluorescence, MR and CT trimodal imaging. *Biomaterials*. 2012;33(4):1079-

1089. doi:10.1016/j.biomaterials.2011.10.039

117. Xing H, Zheng X, Ren Q, et al. Computed tomography imaging-guided radiotherapy by targeting upconversion nanocubes with significant imaging and radiosensitization enhancements. *Sci Rep*. 2013;3:9-11. doi:10.1038/srep01751
118. Liu Q, Sun Y, Li C, et al. F-Labeled Magnetic-Upconversion. 2011;(4):3146-3157.
119. Zhang P, Steelant W, Kumar M, Scholfield M. Versatile photosensitizers for photodynamic therapy at infrared excitation. *J Am Chem Soc*. 2007;129(15):4526-4527. doi:10.1021/ja0700707
120. Hackbarth S, Schlothauer J, Preuß A, Röder B. New insights to primary photodynamic effects - Singlet oxygen kinetics in living cells. *J Photochem Photobiol B Biol*. 2010;98(3):173-179. doi:10.1016/j.jphotobiol.2009.11.013
121. Liu K, Liu X, Zeng Q, et al. Covalently Assembled NIR Nanoplatform for Simultaneous Fluorescence Imaging and Photodynamic Therapy of Cancer Cells. *ACS Nano*. 2012;6(5):4054-4062. doi:10.1021/nn300436b
122. Liu X, Zheng M, Kong X, et al. Separately doped upconversion-C60 nanoplatform for NIR imaging-guided photodynamic therapy of cancer cells. *Chem Commun*. 2013;49(31):3224-3226. doi:10.1039/c3cc41013g
123. Barreto JA, O'Malley W, Kubeil M, Graham B, Stephan H, Spiccia L. Nanomaterials: Applications in cancer imaging and therapy. *Adv Mater*. 2011;23(12). doi:10.1002/adma.201100140
124. Neuberger T, Schöpf B, Hofmann H, Hofmann M, Von Rechenberg B. Superparamagnetic nanoparticles for biomedical applications: Possibilities and limitations of a new drug delivery system. *J Magn Magn Mater*. 2005;293(1):483-496. doi:10.1016/j.jmmm.2005.01.064
125. Yang Y, Qu Y, Zhao J, et al. Fabrication of and Drug Delivery by an Upconversion Emission Nanocomposite with Monodisperse LaF3:Yb,Er Core / Mesoporous Silica Shell Structure. *Eur J Inorg Chem*. 2010;(33):5195-5199. doi:10.1002/ejic.201000778
126. Kennedy LC, Bickford LR, Lewinski NA, et al. A new era for cancer treatment: Gold-nanoparticle-mediated thermal therapies. *Small*.

2011;7(2):169-183. doi:10.1002/smll.201000134

127. Dreaden EC, Mac key MA, Huang X, Kang B, El-Sayed MA. Beating cancer in multiple ways using nanogold. *Chem Soc Rev*. 2011;40(7):3391-3404. doi:10.1039/c0cs00180e
128. Qian LP, Zhou LH, Too HP, Chow GM. Gold decorated NaYF4:Yb,Er/NaYF4/silica (core/shell/shell) upconversion nanoparticles for photothermal destruction of BE(2)-C neuroblastoma cells. *J Nanoparticle Res*. 2011;13(2):499-510. doi:10.1007/s11051-010-0080-6
129. Carrasco E, Del Rosal B, Sanz-Rodríguez F, et al. Intratumoral thermal reading during photo-thermal therapy by multifunctional fluorescent nanoparticles. *Adv Funct Mater*. 2015;25(4):615-626. doi:10.1002/adfm.201403653
130. Zhang Y, Chen B, Xu S, et al. Dually functioned core-shell NaYF4:Er3+/Yb3+@NaYF4:Tm3+/Yb3+ nanoparticles as nano-calorifiers and nano-thermometers for advanced photothermal therapy. *Sci Rep*. 2017;7(1):1-12. doi:10.1038/s41598-017-11897-4
131. Kumar A, Dixit CK. Methods for characterization of nanoparticles. *Adv Nanomedicine Deliv Ther Nucleic Acids*. Published online 2017:44-58. doi:10.1016/B978-0-08-100557-6.00003-1
132. Bazylińska U, Wawrzyńczyk D. Encapsulation of TOPO stabilized NaYF4:Er3+,Yb3+ nanoparticles in biocompatible nanocarriers: Synthesis, optical properties and colloidal stability. *Colloids Surfaces A Physicochem Eng Asp*. 2017;532:556-563. doi:10.1016/j.colsurfa.2017.03.040
133. Li C, Hou Z, Dai Y, et al. A facile fabrication of upconversion luminescent and mesoporous core–shell structured β-NaYF 4 :Yb 3+ , Er 3+ @mSiO 2 nanocomposite spheres for anti-cancer drug delivery and cell imaging. *Biomater Sci*. 2013;1(2):213-223. doi:10.1039/C2BM00087C
134. Li H, Song S, Wang W, Chen K. In vitro photodynamic therapy based on magnetic-luminescent Gd2O3:Yb,Er nanoparticles with bright three-photon up-conversion fluorescence under near-infrared light. *Dalt Trans*. 2015;44(36):16081-16090. doi:10.1039/c5dt01015b
135. Ma J, Huang P, He M, et al. Folic acid-conjugated LaF3:Yb,Tm@SiO2

nanoprobes for targeting dual-modality imaging of upconversion luminescence and X-ray computed tomography. *J Phys Chem B*. 2012;116(48):14062-14070. doi:10.1021/jp309059u

136. Xu S, Yu Y, Gao Y, et al. Mesoporous silica coating NaYF 4 :Yb,Er@NaYF 4 upconversion nanoparticles loaded with ruthenium(II) complex nanoparticles: Fluorometric sensing and cellular imaging of temperature by upconversion and of oxygen by downconversion. doi:10.1007/s00604-018-2965-5
137. Ibuki Y, Toyooka T. Nanoparticle uptake measured by flow cytometry. *Methods Mol Biol*. 2012;926:157-166. doi:10.1007/978-1-62703-2-1_11
138. Huang L, Liu Y. In vivo delivery of rnai with lipid-based nanoparticles. *Annu Rev Biomed Eng*. 2011;13:507-530. doi:10.1146/annurev-bioeng-071910-124709
139. Xu J, Kuang Y, Lv R, et al. Charge convertibility and near infrared photon co-enhanced cisplatin chemotherapy based on upconversion nanoplatform. *Biomaterials*. 2017;130:42-55. doi:10.1016/j.biomaterials.2017.03.041
140. Xiao W, Chen WH, Xu XD, et al. Design of a cellular-uptake-shielding “plug and play” template for photo controllable drug release. *Adv Mater*. 2011;23(31):3526-3530. doi:10.1002/adma.201101806
141. Stone HB, Harding RP. Reversible injury after mild hyperthermia. *Int J Radiat Oncol Biol Phys*. 1986;12(5):823-827. doi:10.1016/0360-3016(86)90042-8
142. Harmon B V., Corder AM, Collins RJ, et al. Cell death induced in a murine mastocytoma by 42-47°c heating in vitro: Evidence that the form of death changes from apoptosis to necrosis above a critical heat load. *Int J Radiat Biol*. 1990;58(5):845-858. doi:10.1080/09553009014552221
143. Issels RD. Hyperthermia adds to chemotherapy. *Eur J Cancer*. 2008;44(17):2546-2554. doi:10.1016/j.ejca.2008.07.038
144. Pérez-Sánchez A, Barrajón-Catalán E, Herranz-López M, Micol V. Nutraceuticals for skin care: A comprehensive review of human clinical studies. *Nutrients*. 2018;10(4):1-22. doi:10.3390/nu10040403
145. Liu Q, Feng W, Yang T, Yi T, Li F. Upconversion luminescence imaging of

cells and small animals. *Nat Protoc*. 2013;8(10):2033-2044. doi:10.1038/nprot.2013.114